Electronic Thesis and Dissertation Repository

4-24-2018 1:30 PM

Simplified Numerical Models in Simulating Corona Discharge and EHD Flows

Sara Mantach
The University of Western Ontario

Supervisor
Adamiak, Kazimierz
The University of Western Ontario

Graduate Program in Electrical and Computer Engineering
A thesis submitted in partial fulfillment of the requirements for the degree in Master of
Engineering Science
© Sara Mantach 2018

Follow this and additional works at: https://ir.lib.uwo.ca/etd

Part of the Electromagnetics and Photonics Commons

Recommended Citation

Abstract

Corona discharge is used in many practical applications. For designing and optimization of corona devices, the discharge phenomenon should be numerically simulated. Most often, the corona discharge model is simplified by neglecting the process dynamics and assuming a limited number of reactions and species. In the extreme case, monopolar corona models with just one species and no reactions are studied. However, there is a problem with determining boundary conditions for the space charge density. The simplest solution to this problem was suggested by Kaptzov, who hypothesized that the electric field on the electrode surface remains constant and equal to the value at the onset conditions, which is known from a semi-empirical Peek's formula. Experimental data confirm good accuracy of this approach. However, it is impossible to experimentally measure the surface electric field at different voltage levels and compare it to Peek's value. Our thesis will discuss different methods for simulating corona discharge in 1D wire-cylinder geometry in air at atmospheric pressure. The classical model based on Kaptzov's hypothesis is compared with other approaches. The first model is still a single-species one, but it uses direct ionization criterion. Two other models consider a higher number of species and some number of reactions, so the ionization layer is included. The surface electric field can differ from Peek's value by almost 43%. In addition, the results of numerical investigations of the EHD flow generated by dc corona discharge in the point-plane configuration in atmospheric air are presented in this thesis. A computational model of the discharge includes the ionization layer and three ionic species. The most important ionic reactions (ionization, attachment, recombination and detachment) are considered. The results of the corona simulations were used to predict the secondary EHD flow. All flow parameters (velocity components, pressure, streamlines) are determined. In addition to main flow vortex reported before, a local vortex near the discharge tip has also been discovered. COMSOL, a commercial finite element package, was used in simulations.

Keywords

Corona discharge, Drift- diffusion equation, Poisson's equation, EHD flow

Dedication

I dedicate this thesis to my mother and father. Hassan and Souad, thank you from the very bottom of my heart for your continuous support and belief in me. I also dedicate this thesis to my nephews who always inspire me to keep moving forward and never lose hope. I as well dedicate this thesis to my two brothers, sister and brother in law. Thank you for your never-ending care. You are all indeed a treasure from God.

Acknowledgments

I am very grateful for my supervisor Prof. Kazimierz Adamiak. Your invaluable help, constant support and clear guidance throughout my research program were truly a blessing. Thank you for your patience and kindness. I really appreciate the chance you offered me to be a part of your research team.

Many thanks to my colleagues Peyman Dordizadeh and Chaoao Shi for the enriching talks we had. I would also like to thank my friends for their support and help. I cannot imagine I could have lived through these couple of years without you.

Table of Contents

List of Tables

List of Figures

Chapter 1

1   Introduction

An introduction to the corona discharge phenomenon, thesis objectives and thesis outline are presented in this Chapter.

1.1   Introduction

In a non-uniform configuration consisting of two or more electrodes, a stable electric discharge, called corona discharge, is produced when a sharp electrode is connected to a high voltage source. The other, much flatter, electrode is usually connected to ground. Because of the difference in the radii of curvature of both electrodes, a high field region is produced near the sharp electrode. If there is an electron in this region, it is accelerated and after reaching sufficient energy it can collide with a neutral molecule detaching another electron, so gas ionization takes place [1]. Positive ions and electrons are produced, and their movement depends on the polarity of the sharp electrode. When electrons leave the high field region, they don't have enough energy to further ionize neutral molecules. In some gases, called electronegative ones, electrons attach to neutral molecules, forming negative ions. Therefore, two regions can be identified in the air gap between both electrodes: a lower field drift region and a high field ionization region [2]. Drift of ions and electrons leads to imposing some momentum on the neutral gas molecules of the host medium, which causes the ionic wind, also known as electrohydrodynamic (EHD) flow.

There exist several forms of corona discharge, which depend on the spatial electrode configuration and the polarity of the applied potential difference, which may be positive or negative. Some of the most common electrode geometries are: needle-plane, wire-cylinder and wire-plane. The discharge for the positive voltage is quite different than the discharge for the negative voltage. In the case of positive corona, as the applied voltage increases, the discharge changes from burst pulse corona, to streamer corona, glow corona and spark discharge. In the case of negative corona, the discharge changes from Trichel pulse corona, to pulseless corona and spark discharge [3].

The major published works on corona discharge may be credited to Loeb, Goldman and Sigmond [2,4]. Loeb analyzed the mechanism of negative corona pulses in air at atmospheric pressure and studied the differences between positive and negative corona currents in air [4]. Robinson was the first to report the existence of ionic wind [5], but Chattok introduced its first quantitative analysis [6]. The lack of complete understanding of the physical processes taking place in corona discharge and important practical applications of this phenomenon make the interest in corona discharge still alive today.

There are many practical applications of corona discharge in industry and research. Some of them are: charging thin insulating films, electrophotography, electrostatic precipitation, removal of gaseous pollutants (mostly NO_x and SO_x) and many others. The electrostatic precipitator was probably the first commercial application of the corona discharge phenomenon and this didn't happen until 1907 [8]. On the other side, corona discharge is harmful in the electrical power systems, where it should be prevented since it causes power loss, produces audible noise and leads to radio interferences [9].

Corona discharge is a complex phenomenon and its experimental investigation is time consuming. Therefore, numerical simulation has been used more and more often. However, due to process complexity some simplifying assumptions are necessary. Despite this, relatively accurate solutions can be still obtained.

1.2   Thesis Objectives

The first objective of this thesis is to perform a numerical investigation of the negative DC corona discharge in atmospheric air in the wire-cylinder configuration. This investigation is done using three different approaches. The first approach includes one ionic species, where two numerical models are tested: one is based on Kaptzov's hypothesis and the other on the direct ionization criterion. The second approach includes three ionic species: electrons, negative ions and positive ions. The final approach in addition to the previous three species includes extra four species: O, O^-, O_3 and $O_2(^1\nabla g)$. The studied geometry consists of a thin wire acting as the corona electrode, which is positioned at the center of a grounded cylinder. The main goal is the determine the electric field on the corona electrode surface, so that a commonly accepted simplifying

assumption, called Kaptzov's hypothesis, can be validated, spatial distribution of electric charge and the current-voltage characteristics.

The second investigated geometry consists of a needle acting as the corona electrode which is perpendicular to a grounded plate. In this model, three ionic species are considered: electrons, positive ions and negative ions. The objective is to investigate a new air flow pattern that has not been reported before in literature on EHD.

To achieve both objectives, the numerical algorithm based on the Finite Element Method was implemented using commercial software COMSOL 5.3. As a result, the distributions of both space charge densities and electric potential can be determined.

Several data sets are reported, including the distribution of electric field on the corona electrode, the spatial distribution of the ionic species and the voltage-current characteristics. In addition to this, three more parameters of interest are presented for the EHD flow. These include the airflow streamlines, the pressure distribution near the corona electrode, and the velocity distribution in the air gap between both electrodes.

1.3   Thesis Outline

The thesis is divided into 6 Chapters. The summary of each Chapter is as follows:

 Chapter 2 includes a summary of some of the previous publications related to numerical simulation of negative corona discharge in wire-cylinder and needle-plate configuration in atmospheric air. Moreover, a review is done on the recent work related to electrohydrodynamic flows. The review covers simulations of one-species, three-species and seven-species corona models. Moreover, the Kaptzov hypothesis and direct ionization criterion are reviewed as well.

Chapter 3 includes the mathematical model and the numerical algorithm for one-species, three-species and seven-species corona discharge models. For the one-species model, two approaches are discussed: one is based on Kaptzov's hypothesis and the other is based on the direct ionization criterion. The equations governing this problem: Poisson's for

electric field and drift-diffusion for the charge transport are presented. In addition, the boundary conditions for all distributions are specified.

Chapter 4 includes the numerical investigation of the DC corona discharge in the wire-cylinder geometry. The electric field and space charge distributions are compared for different numerical models. The validity of Kaptzov's hypothesis is verified.

Chapter 5 includes the simulation results of electrohydrodynamic flow in the point-plane geometry. The three-species model of the corona discharge is investigated first for the stationary discharge model. Determined electric field and space charge density are used to calculate the flow body force. The obtained results predict a double-vortex pattern never reported previously.

Chapter 6 includes a general summary of the thesis and discusses unsuccessful trials to replace some elements of the COMSOL software with specifically written routines.

Chapter 2

2   Literature review

 In this Chapter, a comprehensive literature review is presented regarding the theory and numerical simulation of DC corona discharge and electrohydrodynamic (EHD) flow. This review focuses on two configurations of electrodes: wire-cylinder and needle-plate. Various numerical approaches, from very simplistic to the most advanced are discussed.

2.1   Early Discovery of Corona Discharge

Peek was the first researcher to talk about the appearance of the corona in his book, which he published in 1929 [11]. He discovered that when the voltage between two smooth conductors increases above a certain critical potential, a hissing noise can be heard, a violet light can be observed, if the surrounding medium is dark, and a noticeable reading on a wattmeter is recorded. Peek also noticed the formation of ozone in this process. Moreover, when the air was electrically overstressed, the air constituents, oxygen O_2 and nitrogen N_2, chemically react, leading to the formation of oxides. As a result, the corona discharge is accompanied by the power loss, which has several forms: chemical reactions, noise, light and heat. Peek also reported that the power loss recorded by a wattmeter increases significantly with the increase of the voltage level and also observed the difference between AC and DC corona discharge. The appearance of the AC corona for the positive half-cycle of the supplied voltage is the same as that of the positive DC corona and the same applies to the negative corona. On the other hand, Peek discovered, using a stroboscope, the difference in the discharge pattern in the positive and negative corona discharges. In the case of the negative applied voltage, some reddish beads are formed on the wire. In the case of positive applied voltage, a smoother bluish-white glow is visible.

Moreover, Peek derived an analytical formula, which can be used to calculate the electric field strength E on the active corona electrode at the point of corona onset. Peek took into consideration the air density and the corona electrode radius.

Any geometry that possesses a non-uniform gap can be used for generation of the corona discharge phenomenon. However, in practical situations geometries which have electrodes with significantly different sharpness are more practical. The most commonly studied systems have been the point-to-plane, where the point can be a tip of sharp needle, and the coaxial wire-cylinder systems. In 1965, Loeb explained the difference in the corona pattern between these two systems [12]. While the point-plane geometry has a confined discharge region, in the coaxial geometry the discharge can be initiated at different points on the corona wire.

2.2   Numerical Simulation of Corona Discharge

Numerous electrical, mechanical and chemical processes are associated with the electric corona discharge. To study this phenomenon, major simplifications should be implemented. Even with such simplifications, analytical solutions can't be obtained unless the geometry of the targeted physical problem is one-dimensional. As a result, since the 1960s numerical simulation of corona discharge has been of wide interest to researchers to enhance understanding of industrial and research processes [13]. The two major parameters involved in the simulation of corona discharge are the electric field and the space charge density. These quantities enable the calculation of the electric current, which is in turn the main factor needed for calculation of the power and energy loss. The electric field depends on the space charge magnitude and distribution and the space charge is affected by the electric-field distribution. As a result, both quantities are mutually coupled.

Relevant partial differential equations associated with the electric field and the space charge densities are Poisson's equation for the scalar electric potential and the drift-diffusion equations for all ionic-species. An iterative numerical procedure has been implemented in literature to find the solution of this set of differential equations [14]. The stability and convergence of these methods are highly influenced by the suitable choice of a proper solution algorithm.

2.2.1   Numerical Techniques to Calculate the Electrical Field

The Poisson equation, which governs the electric potential distribution, is a linear partial differential equation of the second order. The techniques for solving this equation can be divided into two groups: differential and integral. The integral methods require the discretization of the active parts of the domain only, which are the electrode surfaces and areas with electric charge. The first integral technique is the Charge Simulation Method (CSM). In this technique, all electrodes are substituted with some number of lumped charges placed inside of the conducting objects. The magnitude of these charges is determined from the condition that the electrode surface should be equipotential. After that, the electric field is calculated by the superposition of the individual electric fields resulting from each point charge. This technique can't be used for nonlinear problems, or for systems having complex geometries, or for infinite electrodes [15].

The second technique uses a similar philosophy and is called the Boundary Element Method (BEM). The unknown in this technique is the surface charge density on the electrode surface, which is determined from the condition of electrode equipotential. These charges physically exist, so the method doesn't rely on artificial charges used in CSM. Mathematically, the method is based on solving integral equations with weakly singular kernels, which makes the approach more complicated. While solution of the Laplace equation (problems without space charge) is relatively fast, problems with space charge are much more time consuming [16].

On the other hand, the differential methods require the discretization of the whole computational domain, which causes problems for open physical problems. The unlimited domains have to be truncated and some artificial boundary conditions need to be imposed, which may be a source of an error. The oldest differential method is the Finite Difference Method (FDM), which is considered the most classical one [17]. As its name implies, the derivatives in the governing partial differential equations are replaced with the finite differences. Although this technique is easy for implementing, it can be complicated for problems having irregular domains. The second differential technique is the Finite Element Method (FEM). Four basic steps summarize FEM: discretizing the computational domain into a specific number of sub-regions called elements, deriving

matrix equations for each element, assembling the element equations and, finally, solving the obtained system of equations where the solution over each element is interpolated using a simple function, most often polynomials. A fine discretization of the domain may lead to large algebraic systems. This technique is easily used to solve problems with complex geometries [18].

2.2.2   Numerical Techniques to Calculate the Space Charge Density

The knowledge of the electric field distribution in a given domain is needed to evaluate the space charge density. One of the most efficient techniques for this purpose is the Method of Characteristic (MOC), where the partial differential equations along the lines, along which the ions move, are reduced to the ordinary differential equations [18]. These lines are called characteristic lines. For single species models these equations have simple analytical solutions. Since it is more difficult to solve a set of ordinary differential equations, application of this technique to the multiple species problems is more problematic.

Another technique, which can be used for the charge transport equations, is the Finite Volume Method (FVM); one of its versions is called the Donor-Cell Method (DCM) [19]. In this method, the domain is tessellated by closed polygonal paths and each polygon has a node enclosed in it. DCM is based on the integral form of the conservation of charges, where each polygon bounds points that are nearer to the node inside the polygon than any other node. This technique can handle problems with multiple species; however, it is time consuming [20].

The third method is FEM which predicts the distribution of space charge in the targeted simulated domain, if the space charge is restricted to the area between the associated electrodes. As discussed before, corona discharge occurs in areas with steep field gradients, which are called ionization regions. Conventional FEM algorithms are often divergent in this case, and to reach a convergent solution, stabilizing techniques should be implemented. One of the stabilizing techniques requires adding the artificial diffusion,

where the physical diffusion coefficient used in the drift-diffusion equations is modified according to the following equation:

$$D_{stabilized} = D_{physical} + \delta h|v| \qquad\qquad (2\text{-}1)$$

where δ is a stabilizing parameter between 0 and 0.5, h is the longest mesh side element and v is the charged species drift velocity. The drawback of such technique is that it adds artificial diffusion in all directions; thus, making it an inconsistent method. The other two consistent methods are the streamline diffusion and crosswind stabilization. Streamline diffusion adds the artificial terms in the direction of the electric field only [7]. This technique is considered consistent because the stabilizing term tends to zero when the solution converges. In the crosswind stabilization an artificial diffusion perpendicular to the electric field lines is added [37]. This technique is used for simulating models which have high electric fields.

Other methods are the Flux Corrected Transport (FCT) and the Total Variation Diminishing technique (TVD). FCT identifies the steep density gradient without introducing any artificial diffusion [63]. It adds an anti-diffusive term to the low-order solution making sure that no new maxima or minima associated with the new added terms are introduced. TVD on the other hand makes sure to eliminate any numerical oscillations which can result from the increase in the flow variables with time. As a result, although the solution can be of the second or third order in the smooth part, it changes to a first order at points where the artificial minima or maxima are generated.

2.2.3   Numerical Investigation of Corona Discharge

Each of the methods mentioned in the previous two sections has some advantages and disadvantages, where each is better for specific applications depending on the problem requirements. In order to handle simulations most efficiently, a combination of numerical methods should be considered, which leads to the idea of hybrid techniques.

In 1985, Morrow was the first to report his work on simulating corona discharge in oxygen and other gases, taking into account a small number of chemical reactions [21]. He used a hybrid technique combining the Flux-Corrected Transport method to solve the

three drift-diffusion equations for ionic species and the FDM method for solving Poisson's equation to determine electric field. A one-dimensional model was considered in this study.

The first published work, which reported using FEM only to simulate corona discharge was authored by Janischewskyj and Gela [18]. They simulated corona in a wire-cylinder configuration assuming a one-dimensional unipolar corona model. Deutsch assumption was satisfied in this simulation since the electrical field is always radial in this configuration [22]. This assumption states that the intensity of the Laplacian field lines changes in the presence of space charge, but the geometry of the lines is preserved.

Abdel-Salam et al. used a hybrid FEM-CSM technique, for simulating corona discharge in wire-to-ground configuration [23, 24]. A monopolar corona model was used where the ionization layer was neglected. They assumed that the electrical field intensity on the corona wire is constant; thus, implementing Kaptzov's hypothesis. Kaptzov's hypothesis states that the electric field on the corona electrode is constant when the applied voltage is above a threshold value, called onset voltage. Chen and Davidson simulated positive and negative corona discharges in a wire-cylinder configuration [25]. A one- dimensional stationary model was adopted, where three ionic species (electrons, negative ions and positive ions) were taken into consideration. FDM was implemented to solve the charge continuity equations and Kaptzov's hypothesis was adopted in this simulation.

BEM and MOC have also been combined to evaluate the electric potential and the charge distribution in 2D models of corona discharge. Adamiak used these two techniques iteratively in order to simulate corona discharge in a wire-duct electrostatic precipitator [26]. Kaptzov's hypothesis was adopted again in this simulation. The numerical results agreed well with the experimental results; however, this hybrid technique was ineffective in terms of computational time. Adamiak and Atten then applied BEM to evaluate the Laplacian electric field, FEM to evaluate the Poisson electric field and MOC to evaluate the space charge [27]. An injection law was applied in this simulation, where the density of the charge carriers on the corona electrode was evaluated from the local electric field value. This technique again satisfied Kaptzov's hypothesis, but in an indirect way.

Accurate results were attained when very fine discretization was used near the corona electrode, since the electric field has a very steep gradient in this area.

Some researchers studied the electric corona discharge using time-dependent and multi-polar models [28]. Liang et al. used a one-dimensional single species model in order to simulate a wire-cylinder electrostatic precipitator under the pulse energization [29]. Rajanikanth and Prabhakar used a two-dimensional single species model to simulate the same problem using a time-dependent model [30]. Salasoo and Nelson used a time-dependent two-dimensional multi-species model in order to simulate a pipe-type precipitator [31].

Many authors investigated negative and positive corona discharge in oxygen, air, SF_6 and other gases taking into consideration more detailed chemistry of ionic reactions. Georghiou et al. simulated corona discharge in a point-plane geometry at radio frequency in air [28]. Detailed models were investigated considering multi-species and taking several ionic processes into account: the ionization of neutral molecules, attachment of electrons, the recombination between negative ions and positive ions and the recombination between electrons and positive ions. Zhang and Adamiak used a similar approach to simulate corona discharge in oxygen in a point-plane geometry, where a DC stationary model was assumed [32].

Yanallah and Pontiga proposed a semi-analytical stationary discharge model in a point-plane configuration for both positive and negative corona discharge in oxygen. The approximate analytical expressions for the electric field and the ionic densities were found by solving the Gauss and the continuity equations. Secondary ionization criterion and photoionization were implemented in the boundary conditions of the problem by using the experimental corona current and applied voltage as inputs [33].

For the cylinder-wire-plate configuration, Dumitran et al. introduced a more realistic non-uniform charge injection that accounts for the field variation on the surface of the ionizing wire of a dual corona electrode [34]. These changes were reported to have a great impact on the ionic current and the space charge distributions.

In 2005, Adamiak et al. came up with a novel approach based on the direct ionization criterion instead of Kaptzov's hypothesis and applied it for a two-dimensional hyperbolic needle-ground configuration. The new approach was compared with two others: one based on Kaptzov's hypothesis and the other one based on the analytical Peek formula with an equivalent electrode radius [60]. BEM, FEM and MOC were combined to solve for the Laplacian electric field, the Poisson component of the electric field and the charge transport equation, respectively. The discharge current was practically the same for the three approaches However, the electric field distributions on the corona electrode surface were slightly different.

2.3   Electrohydrodynamic Flow

Electrohydrodynamic flow (EHD) is the result of the collisions between charged particles, accelerated in the electric field, and neutral gas molecules. This leads to the rise of induced air flow, which has been called the "ion wind".

EHD flow was first observed in 1629 by Cabeo, but the first official acknowledgement was reported in 1709 by Hauksbee [36,37]. Hauksbee discovered that a weak blowing wind is initiated near an electrified body [38]. Cavalo, in turn, provided the first qualitative explanation of the ionic wind [39]. Faraday identified the mechanism responsible for the movement of the air particles between two electrodes, when high voltage is applied to the emitter. He confirmed that ionic wind is driven by the momentum transfer between charged and uncharged particles [40]. In 1873, Maxwell published the most comprehensive work at that time, which is still valid nowadays [41].

Ionic wind generated by the corona discharge has been investigated both experimentally and theoretically, and different models have been investigated. Unipolar ions play the main role in formation of EHD flows; thus, a basic unipolar corona model coupled with Navier-Stokes equation has been adopted by many researches [50,51,52]. Moreover, some researchers have used complex chemical kinetic models of gas discharges to investigate the gas flow [53], but very advanced computational resources were required. Therefore, a fluid model based on three ionic species is considered satisfactory for simulating of ionic wind since it saves computational time [54].

The effect of many factors, including the electrodes geometry, the EHD force and the current-voltage characteristics on the velocity of the ionic wind has been studied. Zhao and Adamiak presented numerical investigation of the EHD flow produced by corona discharge [70]. Three different system configurations were considered with variable applied pressure. The development of the EHD flow to its full pattern has been investigated including the time it takes and the factors that affect it. Improved models were simulated including a set of continuity equations for the charged particles coupled with Poisson's equation [75], where the corona model predicts the distribution of the EHD force and the flow velocity can be then obtained. A fully coupled model including both the continuity equations and the Navier-Stokes equations was proposed by Bérard et al [45]. The numerical investigation involved a steady state simulation of a 2D numerical model.

Some researchers tried to increase the gas flow velocity in a wire-plate configuration without reaching breakdown [56]. In 2014, an empirical model has been proposed linking the ionic wind velocity to the applied voltage and the geometry of the collecting electrode [57]. The measurements of the ions velocity and the discharge current were carried out for different electrode geometries, having a variable air gap length and applied voltage.

Chen et al. have reported the numerical and experimental study of a DC negative corona discharge in a needle-cylinder configuration [54]. They found that the gas near the needle tip flows towards the discharge electrode, while the gas velocity is oriented towards the ground electrode outside the ionization region. Moreover, the EHD force is approximately two orders of magnitude higher in the ionization region than in the drift region.

There exist many applications where ionic wind can be used. The first one is the ionic wind-driven bulk air blowers or EHD pumps. These pumps have several forms where two different flow patterns can be observed: un-ducted flow with an unconstrained manner and ducted flow with a confined manner [47]. The most popular configuration of EHD pump is a sliding discharge-type, where the discharge electrode is a discrete saw-toothed-plate. This configuration allows the generation of high gas velocity compared to a

classical plate discharge electrode [48]. Another configuration is a needle-ring-metal pump. In this configuration, the voltage is applied to both the needle and the ring. As a result, a higher flow velocity is observed [42]. A way to increase the flow velocity is to increase the active area of the pump. This is done by using a serial-staged configuration where a needle array is used [43].

The second application of EHD flow is the boundary layer control. The gas flow produced by the corona discharge is used to change the laminar-turbulent transition regime around obstacles [55]. This is done by changing the velocity in the layer that is very close to the surface of the object. Colver et al. performed a couple of numerical studies on the boundary layer control [73]. One significant aspect is the ion removal and deposition on the plate surface which have a small conductivity. The studies were performed using the Finite Difference Method and a coarse discretization was implemented. Ghazanchaei proposed a model to numerically investigate the electrical and mechanical properties of a unipolar positive corona system around a flat plate by using FEM. He found that the efficiency of the system decreases at higher voltages and that the drag reduction occurs at higher velocities [55].

The third application of EHD flow is EHD drying. EHD drying is the most economical option since the process requires a small pressure difference and a relatively low thermal energy. EHD flow will lead to the dramatic increase of the water mass transfer from the surface of a wet material [74]. Different studies showed that configurations involving multi-pin electrodes have less evaporation rate than single-pin electrodes. Moreover, the spacing between associated electrodes in a multi-wire discharge electrode must be maximized in order to have an optimal drying rate. Shi et al simulated a multiple pin-to-plate configuration and found that the air mass flux is proportional to the voltage and square root of the total current [74].

Chapter 3

3   Mathematical Model and Numerical Algorithm for Simulating Corona Discharge

The corona systems investigated in this thesis consist of two electrodes, one having a much smaller radius of curvature then the other. The system investigated in Chapter 4 is a wire-cylinder configuration and in Chapter 5 it is a needle-plane configuration. In this Chapter, different discharge models are compared and they vary from a single-species to multi-species ones. In the most advanced approach, seven ionic species are considered with electron attachment, avalanche ionization and ionic recombination included. All these models will be used for 1D simulation, while the 2D discharge model is based on the three-species approach only. COMSOL, a commercial finite element package, is used for solving Poisson's equation, governing the electric field distribution, in addition to convection-diffusion equations for all ionic species.

3.1   Single-Species Approach

3.1.1   Idealizing Assumptions

The essential processes in corona discharge are impact ionization of neutral molecules by electrons, attachment of electrons to neutral molecules, recombination of positive and negative ions, and others. The collision of accelerated electrons with gas molecules in the region with strong electric field leads to gas ionization and this takes place near the corona electrode. On the other hand, the presence of electrons in the region where the electric field is low leads to the attachment of these electrons to the neutral gas molecules. As a result, two zones can be identified in the air gap between the electrodes: the ionization zone, where the electron-positive ion pairs are created, and the drift diffusion zone, where negative ions are created. In most engineering applications of the corona discharge the processes in the ionization layer are ignored due to a small thickness of this layer, which is usually in the order of the corona electrode radius of curvature [59]. The most common approaches used in the design and optimization in engineering applications consider only one species of ionic charges moving in electric field with a constant mobility. This single species is injected from the area very near the discharge

electrode and its distribution is predicted by solving the coupled equations of the electric field and the charge transport.

3.1.2   Governing Equations

The first model considers the presence of just one ionic species. This is computationally less expensive than for other models, which consider the presence of three or more ionic species. The Poisson equation for the electric scalar potential is:

$$\nabla^2 V \ = \ -\frac{\rho}{\varepsilon} \qquad\qquad (3\text{-}1)$$

where ε is the permittivity of gas and ρ is the space charge density. The value of the space charge density ρ is calculated by solving the charge transport equation.

In general case, the movement and generation of the ionic species are governed by the following drift-diffusion equation:

$$\nabla\,(-\mu\,\vec{E}n \ - \ D\nabla n) \ = \ R \qquad\qquad (3\text{-}2)$$

where n is the species density $(1/m^3)$, D is the diffusion coefficient (m^2/s), μ is the ion mobility $(m^2/V{\cdot}s)$, R is the source term$(1/m^3{\cdot}s)$, and E is the electric field (V/m).

Since only one ionic species is considered in this model and no ion dissociation and recombination are considered, the source term is equal to zero. The relation between the space charge density ρ and density n is:

$$\rho = e \cdot n \qquad\qquad (3\text{-}3)$$

where e is the electron charge equal to $1.602{\cdot}10^{-19}$ C.

To solve the above equations, appropriate boundary conditions must be formulated. The corona and ground electrodes satisfy Dirichlet boundary conditions for the electric potential:

V= 0 on the ground, and

V= V_c on the corona electrode.

Two boundary conditions are also needed for the charge continuity equation. The first condition is a Neumann condition, where the normal derivative of the space charge density on the collecting electrode is zero. In addition to that, one boundary condition is needed for the space charge density on the corona electrode. Since ionization processes are ignored, the precise value of the space charge density can't be determined. Two criterions were adopted for the boundary condition regarding the space charge density on the corona electrode: Kaptzov hypothesis and direct ionization criterion.

Moreover, in the 2D models, the computational domain is unlimited. In numerical algorithms this domain should be truncated by adding some artificial boundaries. The boundary conditions imposed on these artificial boundaries are: zero charge for the electrostatic potential and zero flux for the charge transport [2]. It is also important that the artificial boundaries should be far enough from the needle tip, so that they wouldn't affect the results.

3.1.2.1   Kaptzov's Hypothesis

According to this hypothesis, at voltages above the onset level, the electric field on the corona electrode remains constant regardless of the voltage level [2]. The electric field for the wire-cylinder configuration in atmospheric air can be calculated from Peek's formula:

$$E_p = 3.1 \cdot 10^6 \left(1 + \frac{0.308}{\sqrt{r}}\right) \qquad (3\text{-}4)$$

where r is the radius of the corona electrode in centimeters, and E_p is the Peek's value in V/m.

For the point-sphere configuration, a different version of Peek's formula should be used:

$$E_p = 3.1 \cdot 10^6 \left(1 + \frac{0.308}{\sqrt{0.5\,r}}\right) \qquad (3\text{-}5)$$

The same formula is commonly used for 2D cases, where the electrode radius is replaced with the sum of principal radii of curvature.

When the electric field is larger than Peek's value, the space charge density should be increased until the electric field is close to this value. On the other hand, when the electric field is smaller than this value, a zero space charge density is assumed on the corona electrode [63].

3.1.2.2   Direct Ionization Criterion

When a free electron, having a sufficiently high energy, hits a neutral gas molecule, a new electron and a positive ion are produced according to the following equation:

$$e + A \rightarrow e + A^+ + e \qquad \qquad (\text{3-6})$$

where A is the atom, A^+ is the positive ion and e is the electron.

This process is called ionization by collision or electron avalanche. If an electric field is applied between two parallel electrodes, electrons are accelerated while traveling from the cathode to the anode due to an action of the electric force. Ionization takes place, if the electron energy is higher than the ionization potential, which is energy needed to dislodge an electron from its atomic shell [58]. If one electron collides with neutral molecules α times per one of centimeter travel and if the initial number of electrons at the cathode is n_0, then the number of the electrons reaching the anode is equal to:

$$N = n_0 \exp{(\alpha\, d)} \qquad \qquad (\text{3-7})$$

where d is the distance between the cathode and the anode and α is called the Townsend's first ionization coefficient.

This process of avalanche ionization would die after some time, because all electrons would be removed from the air gap. A sustained discharge requires new seed electrons generated by other mechanisms. Two the most important are photoionization and secondary emission. Photoionization takes place when UV radiation, generated by some ionic reactions, absorbed by a molecule is larger than the ionization potential. UV
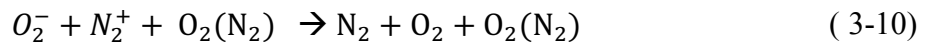
radiation is propagated in all direction and is not affected by the electric field, so photoionization can generate ions at points of higher electric potential (in some sense it travels against electric field) and this can lead to sustained discharge.

On the other hand, secondary ionization is a process of ejecting electrons from the discharge electrode. The positive ions produced by the avalanche ionization are attracted towards the cathode electrode. If the energy of the positive ion is greater than double the cathodic metal work function, one electron is released to gas and a second electron neutralizes the positive ion. The released electrons are called secondary electrons and they are the source electrons for the next avalanches. The probability of this process is associated with Townsend's secondary ionization coefficient γ. Like α, γ is the net number of secondary electrons produced by one positive ion and its value depends on the gas pressure, ion velocity and the material of the electrode.

3.2   Three-Species Approach

3.2.1   Governing Equations

This model takes into consideration four chemical reactions including the electron avalanche ionization, the ionic recombination of the electrons and the positive ions, recombination of the positive and negative ions, and the electron attachment to neutral molecules [8]:

$$e + O_2 \rightarrow 2e + O_2^+ \tag{3-8}$$

$$e + O_2^+ (N_2^+) \rightarrow O_2(N_2) \tag{3-9}$$

$$O_2^- + N_2^+ + O_2(N_2) \rightarrow N_2 + O_2 + O_2(N_2) \tag{3-10}$$

$$e + O_2 \rightarrow O_2^- \tag{3-11}$$

As a result, the model consists of four partial differential equations and boundary conditions for all equations. The first three equations are the drift-diffusion equations in which the generation, dissipation and movement of the ionic species are considered. The

fourth equation is Poisson's equation, which is used to calculate the electric potential distribution:

$$\nabla(-\mu_e \vec{E} n_e - D_e \nabla n_e) = R_e \qquad (3\text{-}12)$$

$$\nabla(\mu_p \vec{E} n_p - D_p \nabla n_p) = R_p \qquad (3\text{-}13)$$

$$\nabla(-\mu_n \vec{E} n_n - D_n \nabla n_n) = R_n \qquad (3\text{-}14)$$

$$\nabla^2 V = -\frac{e(n_p - n_e - n_n)}{\varepsilon} \qquad (3\text{-}15)$$

where n_e, n_p, n_n are the densities ($1/m^3$) of electrons, positive ions and negative ions, respectively, D_e, D_p, D_n are the diffusion coefficients (m^2/s), μ_e, μ_p, μ_n are the mobilities ($m^2/V \cdot s$), R_e, R_p, R_n are the source terms ($1/m^3 \cdot s$), and E is the electric field (V/m). The values of these parameters have been determined experimentally and are given in Table 3-1 [66].

Table 3-1: Swarm parameters for the ionic reactions in oxygen

Parameter	Value	Unit
Electron mobility (μ_e)	$1.9163 \cdot E^{-0.25}$	[$m^2/V \cdot s$]
Positive ion mobility (μ_p)	$2.43 \cdot 10^{-4}$	[$m^2/V \cdot s$]
Negative ion mobility (μ_n)	$2.7 \cdot 10^{-4}$	[$m^2/V \cdot s$]
Electron diffusivity (D_e)	0.18	[m^2/s]
Positive ion diffusivity (D_p)	$0.028 \cdot 10^{-4}$	[m^2/s]
Negative ion diffusivity (D_n)	$0.043 \cdot 10^{-4}$	[m^2/s]
Recombination coefficient of positive and negative ions (β_{np})	$2 \cdot 10^{-13}$	[m^3/s]

Recombination coefficient of electrons and positive ions (β_{ep})	$2 \cdot 10^{-13}$	$[m^3/s]$
Ionization coefficient (α)	$3.5 \cdot 10^5 \cdot \exp(-1.65 \cdot 10^7/E)$	$[1/m]$
Attachment coefficient (η)	$1.5 \cdot 10^3 \cdot \exp(-2.5 \cdot 10^6/E)$	$[1/m]$

As seen in Table 3-1, the ionization reaction rate coefficients are expressed by using the local electrical field approximation. The following terms represent the reaction rates in equations for electrons, positive ions and negative ions:

$$R_e = \alpha\, n_e\, \mu_e\, \vec{E} - \eta\, n_e\, \mu_e\, \vec{E} - \beta_{ep}\, n_e\, n_p \qquad (3\text{-}16)$$

$$R_p = \alpha\, n_e\, \mu_e\, \vec{E} - \beta_{ep}\, n_e\, n_p \qquad (3\text{-}17)$$

$$R_n = \eta\, n_e\, \mu_e\, \vec{E} - \beta_{np}\, n_n\, n_p \qquad (3\text{-}18)$$

In order to have a self-sustained corona discharge model, some mechanism for generating seed electrons must be implemented. The most important source of these electrons is the secondary emission from the discharge electrode. When the positive ions collide with the negative corona electrode, the secondary electrons are ejected. The concentration of the secondary electrons is given by the following equation [72]:

$$n_e = \gamma \cdot n_p \cdot \frac{\mu_p}{\mu_e} \qquad (3\text{-}19)$$

where n_e is the concentration of the electrons on the corona wire ($1/m^3$). The secondary emission coefficient γ is taken to be 0.001.

3.3   Seven-Species Approach

3.3.1   Governing Equations

The complexity of the investigated model can be increased from a simple three chemical species model into a more complicated one, containing seven chemical species and twelve chemical reactions. In the previous model, only electrons, positive and negative

ions were included, which is usually acceptable in a typical electrical model. A new model has been extended to include not only the attachment of electrons to the neutral oxygen molecules, but also the dissociative attachment reaction as follows:

$$e + O_2 \rightarrow O + O^-$$ (3-20)

As a result, the fourth and fifth chemical species are introduced, which are the atomic oxygen O and the corresponding atomic oxygen negative ion O⁻ . Two more reactions including the source and sink of the atomic oxygen should be introduced correspondingly

$$e + O_2 \rightarrow O + O + e$$ (3-21)

$$O + O \rightarrow O_2$$ (3-22)

For a more realistic model, ozone should also be added as the sixth chemical species. The reason behind this is that the atomic oxygen is very active according to the following equation:

$$O + O_2 \rightarrow O_3$$ (3-23)

The sink source of the ozone is presented in the following chemical reaction:

$$e + O_3 \rightarrow O_2 + O + e$$ (3-24)

The last chemical species included in the model is the excited oxygen $O_2(^1\nabla_g)$. This species is an important component in the production of ozone. The second sink source of the ozone is represented in the following equation:

$$O_2 (^1\nabla g) + O_3 \rightarrow O_2 + O_2 + O$$ (3-25)
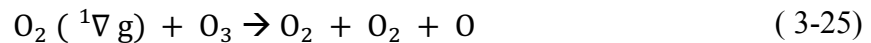
On the other hand, the source term of the excited oxygen is presented in the following equation:

$$e + O_2 \rightarrow O_2 (^1\nabla g) + e$$ (3-26)

The rate coefficients of all the reactions included in this section are specified according to the experimental data compiled by Kogelschatz [68]. These coefficients are presented in tables as a function of the reduced electric field expressed in T_d. T_d is the physical unit of the ratio E/N, where E is the electric field expressed in V/m and N is the concentration of neutral molecules expressed in $1/m^3$. As before, the local field approximation is used.

In the previous model, the number density of oxygen molecule O_2 was assumed to be constant. This assumption can't be preserved in this model. The reason is that the atomic oxygen and ozone are being taken into consideration and their concentration is relatively high. Thus, the number of oxygen molecules decreases in accordance to the production of the atomic oxygen and the ozone.

Because the atomic oxygen, ozone and the excited oxygen species are not moved by the electric field, the diffusion equation for these species, in which the generation and diffusion are considered, is as follows:

$$\nabla \left(- D_i \nabla n_i \right) = R_i \qquad\qquad (3\text{-}27)$$

3.4   Numerical Algorithm

3.4.1   Numerical Algorithm for Single-Species Models

Simultaneous computation of both the space charge and potential distribution is needed to simulate the corona discharge. The numerical algorithm for simulating the corona discharge in the wire-cylinder configuration is based on the Finite Element numerical technique implemented in the COMSOL commercial software. The value of the charge density on the corona wire is a parameter which should be determined using two criteria: one based on Kaptzov's hypothesis and another using the direct ionization condition.

In the model using Kaptzov's hypothesis, a MATLAB function is used to update the surface charge density until the electric field on the corona electrode surface is approximately equal to that resulting from the Peek's formula. This is achieved by implementing an iterative process in which the charge density is modified using the following formula [62]:

$$\rho_{i+1} \ = \ \rho_i \ + \ K \cdot (E_i - E_{onset}) \hspace{3cm} (3\text{-}28)$$

where ρ_i and E_i are the surface charge density and the surface electric field, respectively, E_{onset} is the onset value and K is an experimental constant, which represents the step increase inside the MATLAB routine. If K is too small, more iterations are needed to reach convergence. On the other hand, divergence takes place, if K is too big.

The second approach is based on the direct ionization criterion, in which the condition for a self-sustained corona discharge links both γ and α_{eff} by the following formula [60]:

$$\int \alpha_{eff(r)} \ dr = \ln(1 + \frac{1}{\gamma}) \hspace{3cm} (3\text{-}29)$$

where α_{eff} is the effective ionization coefficient, which is equal to the difference between the attachment and the ionization coefficients.

If the gas involved in the simulation is air, the effective ionization coefficient α_{eff} can be expressed as [64]:

$$\alpha_{eff}(E) = A \, p \, [\, (\frac{E}{E_0})^2 - 1] \hspace{3cm} (3\text{-}30)$$

where A= 48.5 1/(cm·atm) and $E_0/p = 3.1 \cdot 10^4$ V/(cm·atm).

A MATLAB function is used to evaluate the integral and compare it to the right-hand side of (3-29). If the integral is larger or smaller than the right-hand side, space charge is increased or decreased, respectively.

3.4.2   Numerical Algorithm for Multispecies Models

FEM is used to solve Poisson's equation and the three drift-diffusion equations via the commercial software COMSOL. The modules: "Electrostatics" and "Transport of diluted species" are used to solve for the electric field and the space charge densities of the three-ionic species, respectively. According to [67], the most challenging part of simulating corona discharge is the equation of the charge transport. To have a stable numerical

algorithm, under-relaxation of the ionic species densities needs to be incorporated in the iterative algorithm. This is done by modifying the species concentrations numerically using the following equation:

$$n_{new} = n_{old} + \alpha (n_{current} - n_{old}) \qquad (3\text{-}31)$$

α falls in the range between 0.1 and 0.8. The value of α affects the number of iterations needed for convergence. For low voltage levels, a faster convergence is reached when α has an initial value of 0.8 for the first couple iterations. α is reduced sequentially to 0.6, 0.4 and 0.2 until convergence is obtained for α=0.1. For high voltage levels, high values of α lead to a divergent solution. Accordingly, α is set to 0.1.

In the case of seven-species model, additional four transport of diluted species modules are added in COMSOL to represent the four-chemical species: O, O^-, O_3 and $O_2(^1\nabla_g)$. These additional modules don't require under-relaxation technique.

3.5   Governing Equation for the EHD Flow

EHD flow is generated when ions, drifting in electric field, collide with neutral molecules. There is a momentum transfer, which causes gas motion. When this EHD flow is simulated, in addition to solving the Poisson's equation for electric field and the drift-diffusion equations for transport of ionic species, an additional equation is needed for the airflow. The Navier-Stokes equation is as follows:

$$\rho_f (u.\nabla)u = -\nabla P + \eta \nabla^2 u + \vec{F} \qquad (3\text{-}32)$$

where ρ_f is the fluid density (kg/m³), P is the pressure (P), η is the fluid viscosity (kg/ms) and $\vec{F}$ is the Coulomb force. The electric Coulomb force is the main factor leading the EHD flow:

$$\vec{F} = q\vec{E} \qquad (3\text{-}33)$$

For the boundary conditions, the needle body and the ground plate are defined as the stationary walls, where the velocity vector is equal to zero.

3.6   Conclusions

In this Chapter, different models for simulating electric corona discharge have been discussed and they varied from one-species to three-species and finally seven-species ones. In the single species models, the ionization zone is neglected, and two kinds of boundary conditions were implemented for the space charge density: one based on Kaptzov's hypothesis and the other based on the direct-ionization criterion. In the three-species model, four chemical reactions are taken into account. In the seven-species model, an additional seven chemical reactions are considered. For each model, proper boundary conditions have been imposed. The numerical algorithms have been reviewed. The three-species model needed the under-relaxation technique to have a stable simulation. The numerical investigation was performed with the aid of the COMSOL commercial software.

Chapter 4

4 Validation of Kaptzov's Hypothesis for Wire-Cylinder Configuration in Air

The results of numerical investigations of the dc corona discharge in a wire-cylinder configuration in air at atmospheric pressure are presented in this Chapter. Four different discharge models are compared, including single-species, three-species and seven-species ones. For the single-species models, two approaches are tested: one based on Kaptzov's hypothesis and the other one based on the direct ionization criterion. The simulation results for the total corona current and the electric field on the corona electrode surface for different discharge models are compared with that of the single-species corona discharge model based on Kaptzov's hypothesis.

4.1 Description of the Model

Negative DC corona discharge has been investigated in a 1D axisymmetric wire-cylinder geometry considering only a single species of ionic charges, which can be treated as a negative ion. The investigation is carried out in air at atmospheric pressure and room temperature. The wire, which has a radius of R_1=100 μm, is placed coaxially with a grounded cylinder of radius R_2 =3 cm. In the simulated configuration, the Peek's value is E_p =12.4 MV/m and the corona onset voltage is equal -7.2 kV. The domain has been non-uniformly discretized into 4000 elements with an element length increase of 1% when getting away from the corona electrode. Simulations were carried out for negative DC voltages supplied to the wire in the range of -7.2 kV to -12 kV with a 500V step. The only parameter, which characterizes ion drift is the ion mobility, which is assumed to be equal to $2.4 \cdot 10^{-4}$ m^2/(V·s). The air permittivity was equal to $\varepsilon = \varepsilon_0$.

4.2 Single-Species Model

Figure 4-1 shows the electric field in logarithmic scale along the air gap between the two electrodes for three voltage levels: -8.7 kV, -9.7 kV and -10.7 kV, calculated from the model based on Kaptzov's hypothesis and the direct ionization criterion. It can be seen that the electric field calculated from the model applying direct ionization criterion is

larger than that based on Kaptzov's hypothesis. The reason behind this is the restriction imposed on the model applying Kaptzov's hypothesis, where the electric field must be equal to Peek's value. The model based on the direct ionization criterion doesn't have this restriction and the electric field on the corona wire surface at different voltage levels slightly varies.
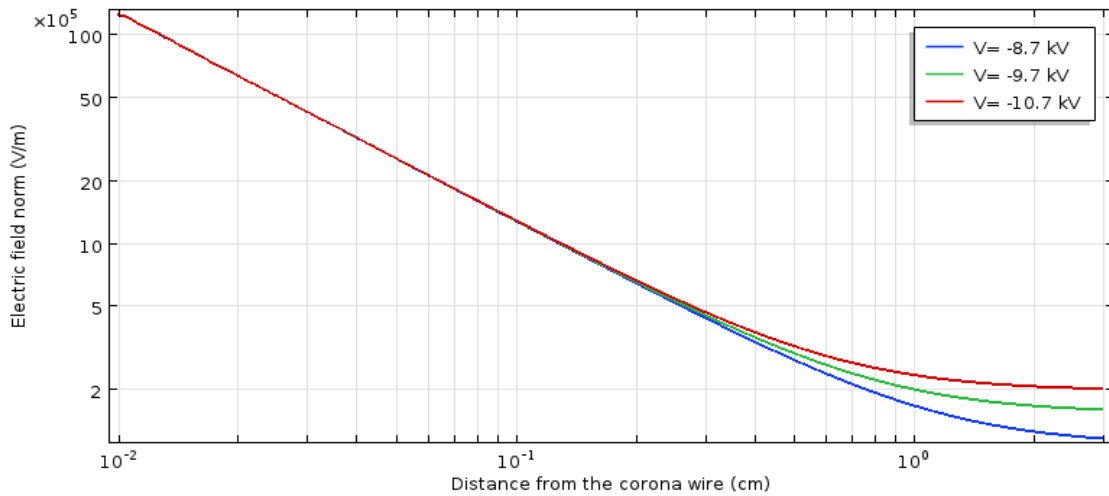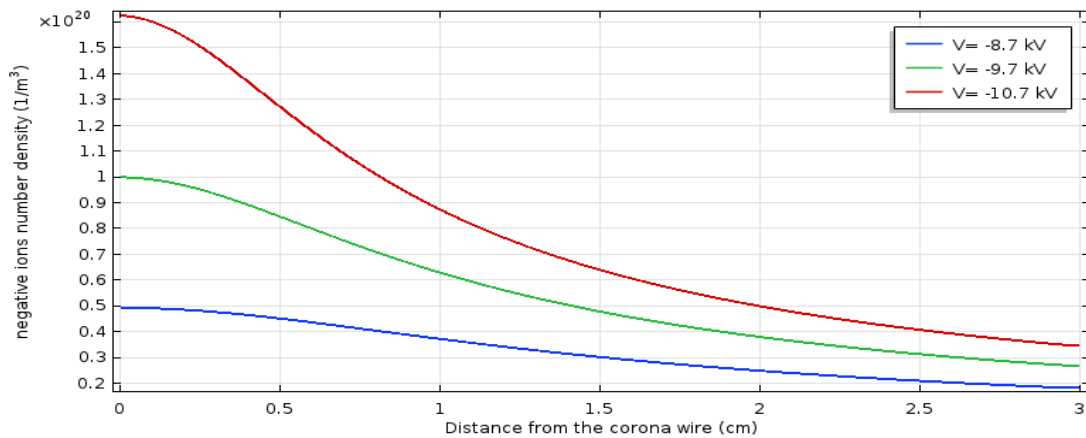

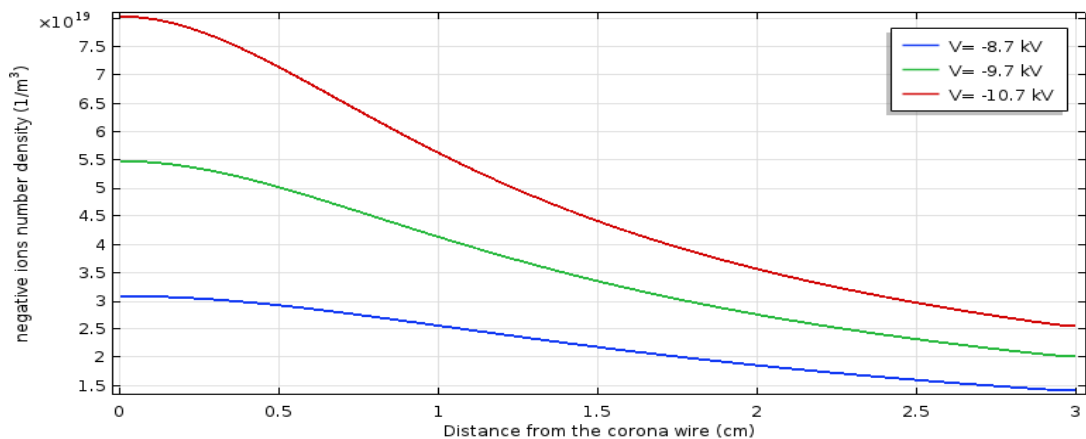a) Electric field calculated from the model applying Kaptzov's hypothesis
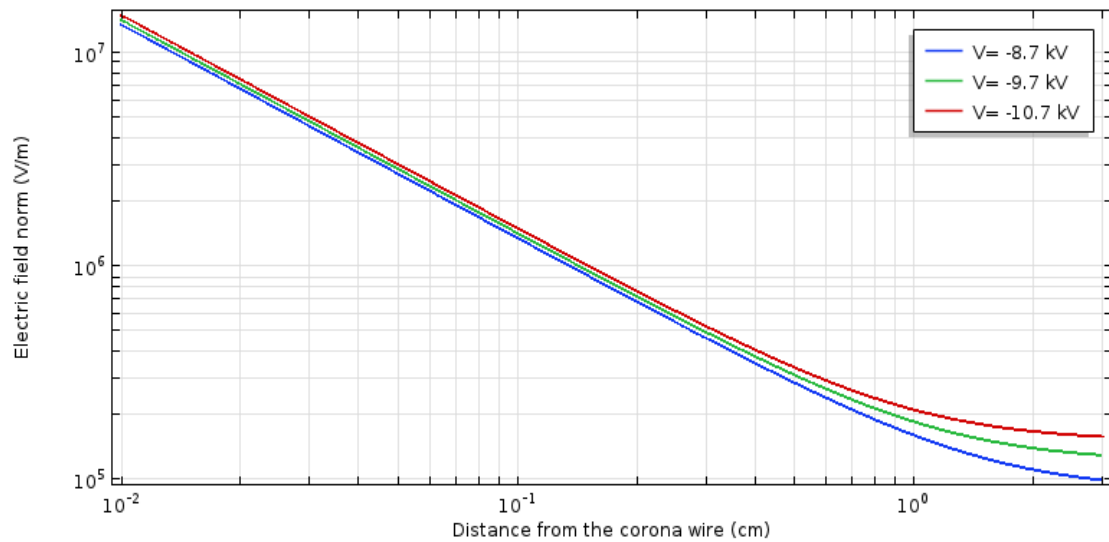
b) Electric field calculated from the model applying direct ionization criterion

Figure 4-1: Electric field in the air gap between electrodes at three different voltage levels for the single species models

Figure 4-2 shows the space charge density distribution along the radial direction at three different voltages: -8.7 kV, -9.7kV and -10.7kV for both investigated models. For all voltage levels, most of the space charge density concentrates near the corona electrode. The concentration decreases until it reaches a very low value near the collecting electrode. The space charge concentrated near the corona electrode is larger in the model based on Kaptzov's hypothesis. The difference in the space charge density calculated from the model applying Kaptzov's hypothesis and the direct ionization criterion increases as the voltage level increases.

a) Space charge density for the model applying Kaptzov's hypothesis

b) Space charge density for the model applying direct ionization criterion

Figure 4-2: Space charge density distribution at three different voltage levels for the single species models

Figure 4-3 shows the total number of the ionic species for different voltages calculated from the models based on the direct ionization criterion and Kaptzov's hypothesis. The total number of the ionic species for the model using direct ionization approach is smaller than the number obtained from the model using Kaptzov's hypothesis. As the corona wire voltage increases, the difference between the total number of negative ions resulting from the two models increases until it reaches 53% at -15 kV. Since the electric field resulting from Kaptzov's hypothesis is lower than that resulting from direct-ionization criterion, more negative-ions are accumulated in the airgap in this model. Charges accumulated closer to the ground electrode have smaller effect on the surface electric field, so a very large difference in the overall number of ions has relatively small effect on the electric field.
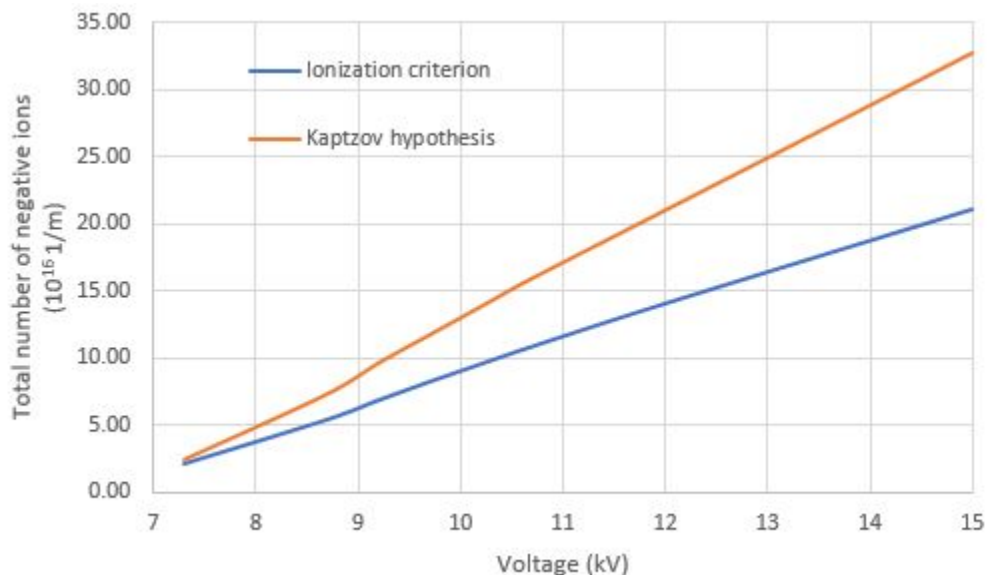
Figure 4-3: Total number of negative ions for different voltage levels from the model using Kaptzov's hypothesis and the direct ionization criterion.

4.3   Three-Species Model

The single species corona discharge simulation has been extended to a three-species model, which includes electrons, negative ions and positive ions. A stationary model has been investigated. The voltage-current curve, the electron and ionic species number densities and the electric field distribution for different voltages are presented.

Table 4-1 shows the maximum concentration for the three-ionic species present in this model for different voltage levels. As the voltage increases, the densities of different ions increase.

Table 4-1: Maximum number densities of different species for different voltage levels

Voltage (kV)	Maximum electron concentration ($1/m^3$)	Maximum positive ion concentration ($1/m^3$)	Maximum negative ion concentration ($1/m^3$)
7.3	$5.94 \cdot 10^{12}$	$1.46 \cdot 10^{15}$	$4.62 \cdot 10^{14}$
8	$1.06 \cdot 10^{13}$	$2.59 \cdot 10^{15}$	$8.14 \cdot 10^{14}$
8.7	$1.61 \cdot 10^{13}$	$3.93 \cdot 10^{15}$	$1.22 \cdot 10^{15}$
9.7	$2.53 \cdot 10^{13}$	$6.19 \cdot 10^{15}$	$1.90 \cdot 10^{15}$
10.7	$3.56 \cdot 10^{13}$	$8.81 \cdot 10^{15}$	$2.67 \cdot 10^{15}$
12	$5.19 \cdot 10^{13}$	$1.28 \cdot 10^{16}$	$3.78 \cdot 10^{15}$
15	$9.27 \cdot 10^{13}$	$2.26 \cdot 10^{16}$	$6.54 \cdot 10^{15}$

Furthermore, the spatial distributions of all ionic species for two voltage levels: -8.7 kV and -15 kV, are presented in Figure 4-4. As it can be seen from this Figure, electrons and negative ions migrate towards the ground electrode while the positive ions are

concentrated near the corona electrode. It is also obvious that the number density of all ions increases as the voltage increases. The exponential increase in the concentration of the electrons near the discharge electrode is caused by the avalanche ionization. This is represented by a linear curve in the log scaled plots. The maximum electron concentration is reached at approximately the edge of the ionization layer. Starting from that point, the electron concentration starts to decrease, as electrons are attached to neutral molecules.

Positive ions should not exist outside of the ionization layer. However, the numerical model predicts a smooth continuous distribution, so some concentration is predicted there. However, this concentration is a few orders of magnitude smaller and negligible from the practical point of view.

The concentration of negative ions is equal to zero on the discharge electrode. Near the discharge electrode it increases because of the attachment of electrons to neutral molecules. Starting from some point in the domain, this concentration starts to decrease as no new ions are generated and the total number of ions is distributed over an increasing area.

a) Electron distribution
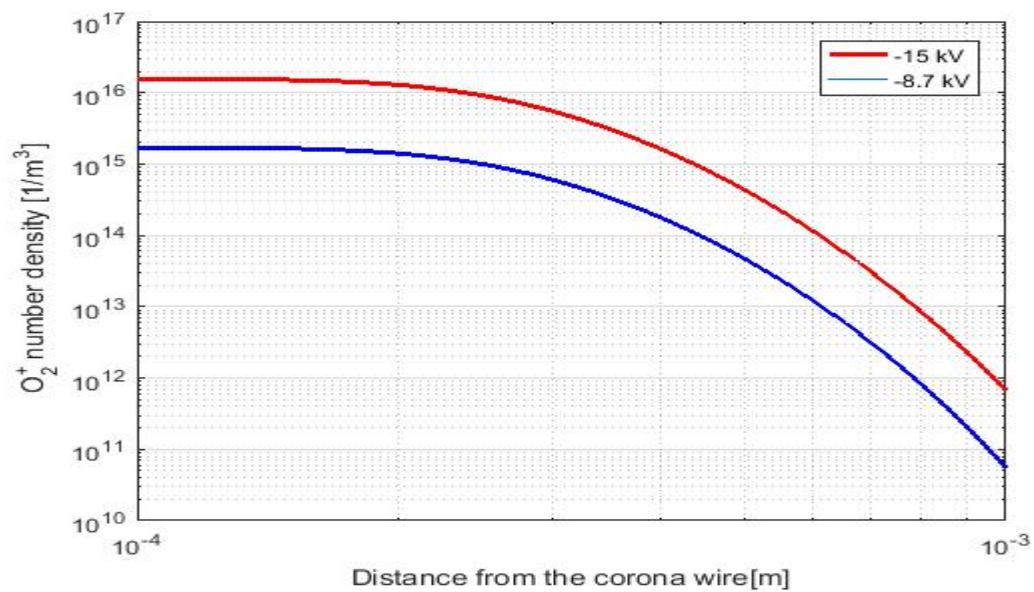
b) Positive ions distribution
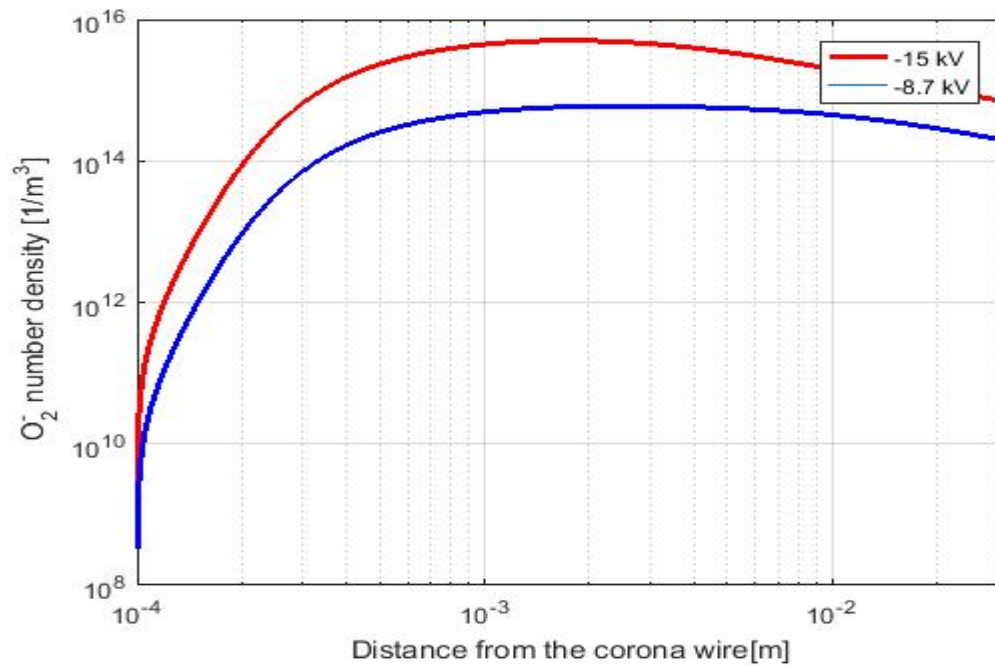
c) Negative ions distribution

Figure 4-4: Ionic species distribution for voltage levels of -8.7 kV and -15 kV

4.4   Seven-Species Model

The distribution of the chemical species has been investigated for different voltage levels and it shows the same trend regardless on voltage. These distributions were in close agreement with the results published by Castellanos et al. [69]. Figure 4-5 shows the distribution of the different species for voltage levels of -8.7 kV and -15 kV.
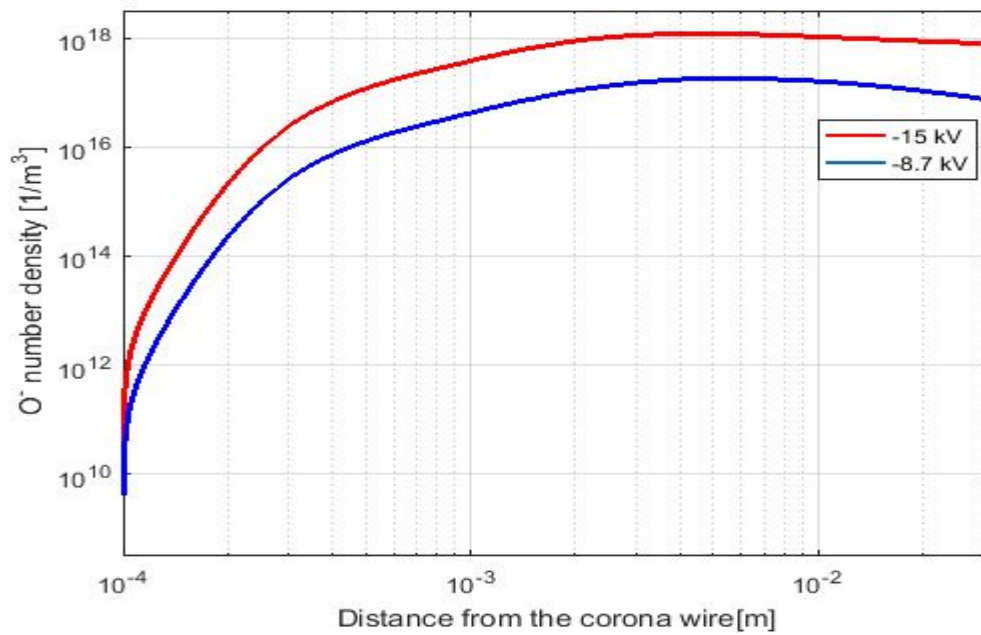
a) Distribution of O⁻
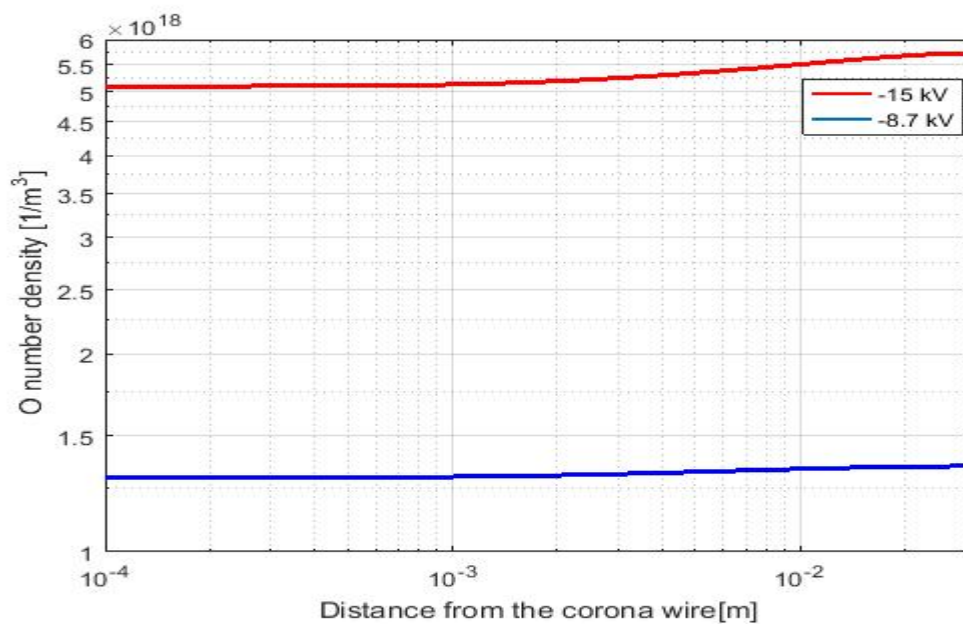
b) Distribution of O
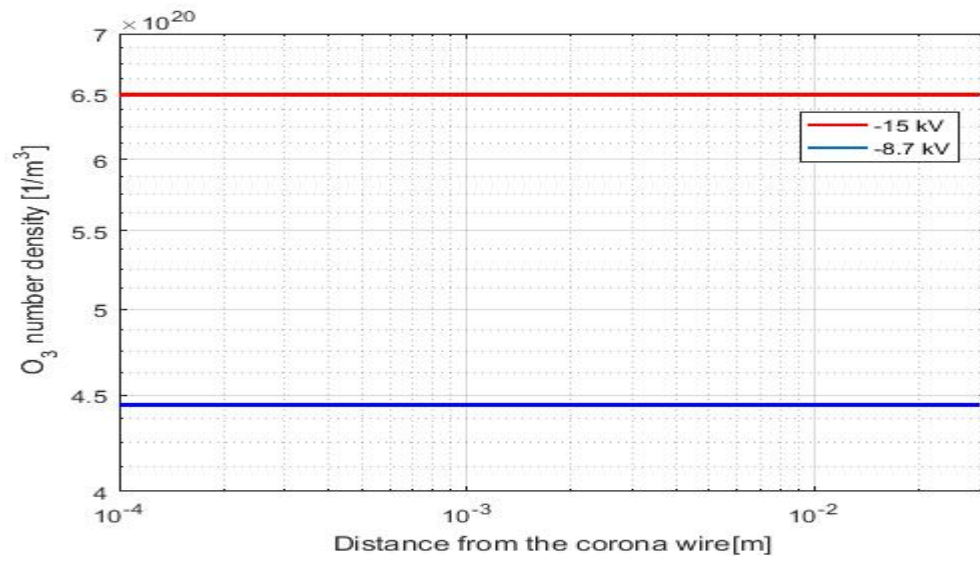
c) Distribution of O₃
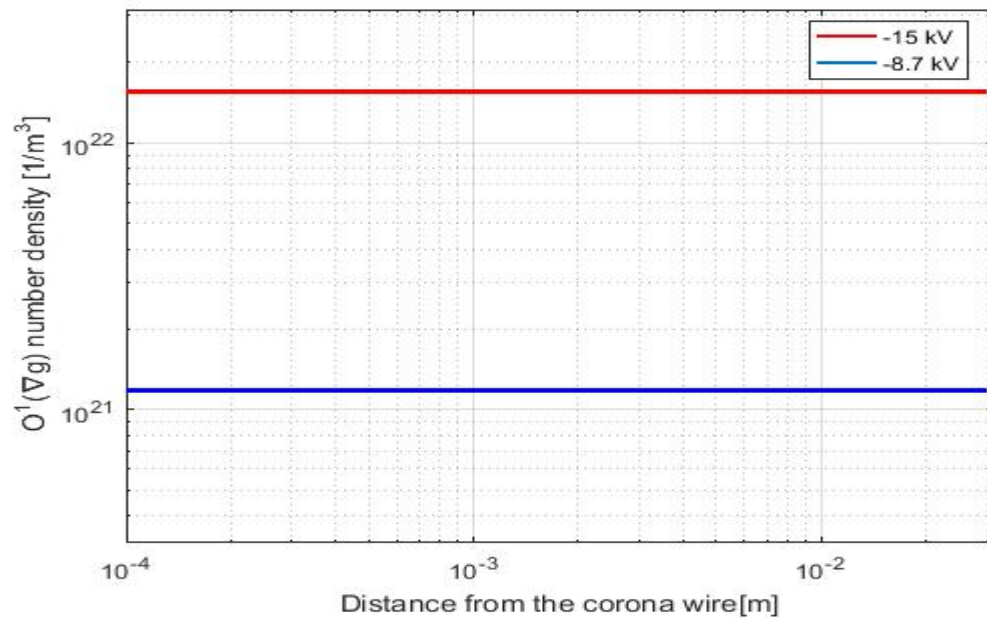
d) Distribution of $0^1(\nabla_g)$

e) Distribution of $0_2{}^+$
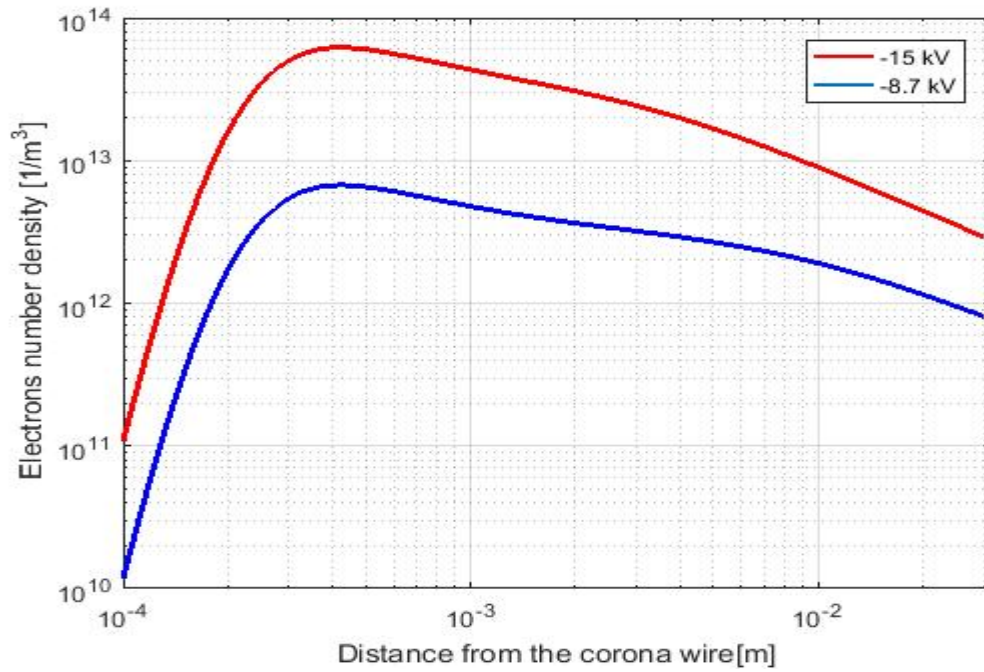
f) Distribution of electrons
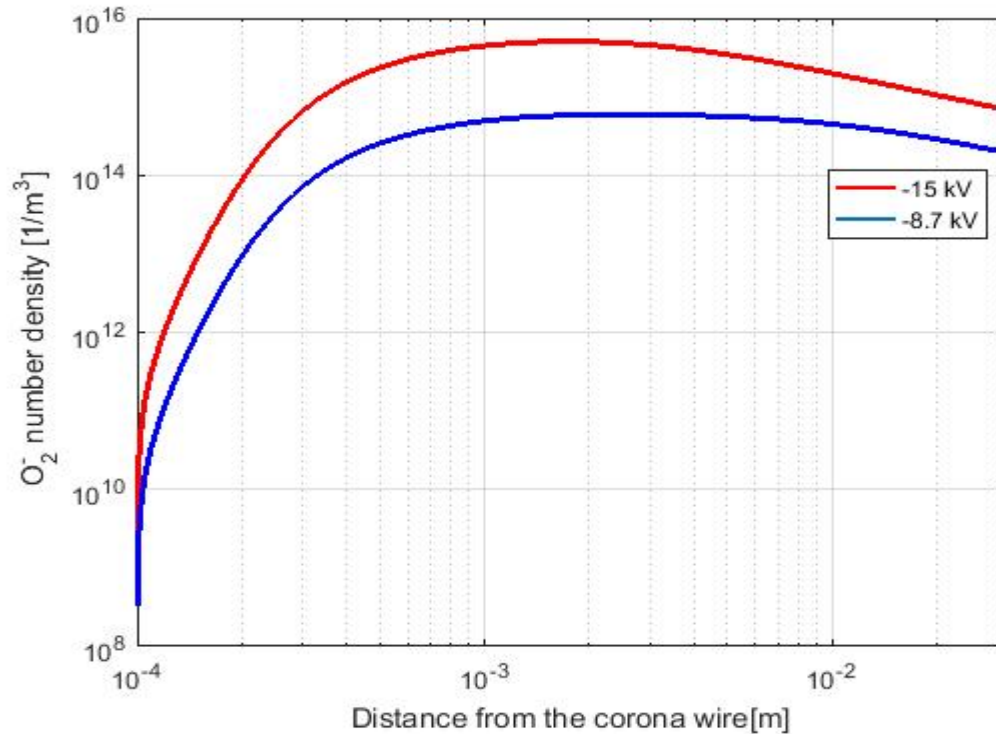
g) Distribution of O_2^-

Figure 4-5: Ionic species distribution of seven-species model for voltages -8.7 kV and -15 kV

Distribution of electrons, and positive and negative O_2 ions for this model is not much different than for the three-species model. One new charge species, O⁻, shows a distribution similar to O2-. There are also three neutral species (O, O_3 , $0^1(\nabla_g)$) and their motion is affected by diffusion only. In this situation a uniform distribution would be expected. A slightly non-uniform distribution in one case is caused by numerical errors.

The thickness of the ionization layer can also be evaluated from the ionic species distributions of the multipolar models: the loss of electrons due to attachment reactions balances the production of electrons due to ionization. Considering the concentration of the positive ions indicates that the thickness of the ionization zone is about 200 μm.

4.5   Electric Field at the Corona Wire

At the onset level, the electric field is high enough for the corona discharge to take place near the corona electrode and all discussed models should predict a very similar value. Figure 4-6 shows the electric field on the corona electrode surface for different voltage levels calculated from different numerical methods. In the case of Kaptzov's hypothesis, the electric field at the corona electrode should be theoretically the same for any wire voltage. Practically, the values diverge from Peek's value by about 1.6% due to numerical errors. In the case of the model applying the direct ionization criterion, the electric field at the onset voltage is higher by 2% than Peek's value. As the voltage increases, the electric field at the corona wire increases until it diverges from Peek's value by 43.56% for the voltage of -15 kV. For the multi-species models, the difference between the electric field intensity predicted from the seven- and the three-species models are negligible so the two graph lines overlap. At lower voltages, the electric field calculated from multi-species model is about 2% higher than Peek's value; it satisfies Peek's formula for voltages higher than -8.3 kV.
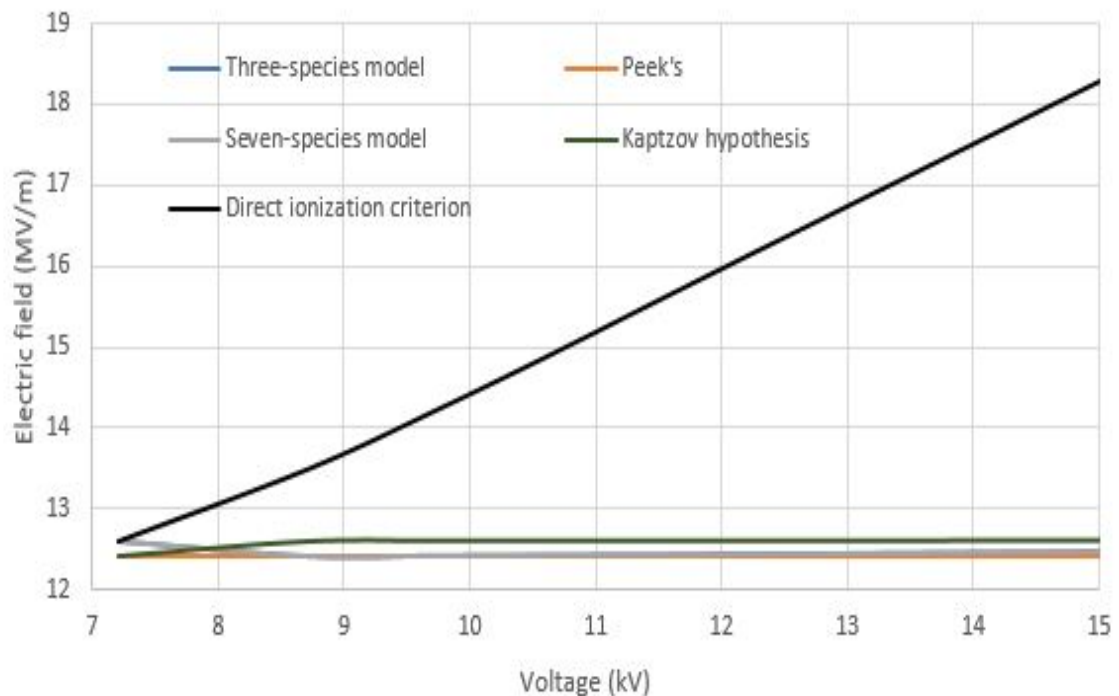
Figure 4-6: Electric field on the corona wire for the four investigated models

4.6   V-I Characteristic Curves

Sato proposed a method to calculate the corona discharge current [61]. This formula is derived from the motion of charged particle between electrodes, and it depends on the energy balance equation.

$$I = \frac{1}{V} \int 2\pi r \, \mu_n \, \rho \, \vec{E}.\overrightarrow{E_L} \, dr \tag{4-1}$$

where μ_n is the ion mobility (m^2/V·s), ρ is the space charge (C/m^3) , V is the applied voltage on the corona wire, $\overrightarrow{E_L}$ is the Laplacian electric field (V/m), $\vec{E}$ is the actual electric field (V/m) , I is the current (A/m) and the integration is done over the radial line connecting both electrodes.

The current in the stationary single-species case can be also calculated by integrating the current density (A/m^2), equal to $\rho\mu_n E$, on the electrode surface. However, in the 1D case, no integration is needed. As a result, the total current is is equal to:

$$I = 2\pi R_1 \mu_n \rho E \tag{4-2}$$

The currents resulting from applying equations (4-1) and (4-2) are the same.

To calculate the discharge current for the three-species model, some modifications need to be done to Sato's equation to account for the added electrons and positive ions species.

$$I = \frac{1}{V} \int 2\pi r (\mu_e n_e + \mu_p n_p + \mu_n n_n) \, \vec{E}.\overrightarrow{E_L} \, dr \tag{4-3}$$

The formula for calculating the discharge current should be further expanded to include the ionic species O⁻ in the case of the seven-species model. As a result, Sato's formula is as follows:

$$I = \frac{1}{V} \int 2\pi r (\mu_e n_e + \mu_p n_p + \mu_n n_n + \mu_{O^-} n_{O^-}) \, \vec{E}.\overrightarrow{E_L} \, dr \tag{4-4}$$

At the onset level, the current is zero. As the applied voltage on the corona electrode increases, the discharge current starts building up in a parabolic manner. More

specifically, the corona current is proportional to V· (V-V$_{onset}$). Figure 4-7 shows the currents resulting from the four investigated models. The difference in the current resulting from Kaptzov's hypothesis and the current obtained from a model using the direct ionization criterion is negligible. Until the voltage -8.3 kV, both currents are the same. Above this voltage, the current resulting from applying Kaptzov hypothesis increases at a higher rate than the current resulting from applying the direct ionization criterion and the difference reaches 1.25 mA/m at the voltage level -15 kV.

The currents resulting from the three-species and seven-species models are very close and the difference is below 0.1%. As a result, both curves overlap on the graph.

On the other hand, the values of the discharge current for different voltage levels obtained from the multipolar models are much higher than the values obtained from the monopolar models. The difference between the currents resulting from the multipolar and monopolar models increases as the applied voltage increases until it reaches a maximum difference of 2 mA/m.
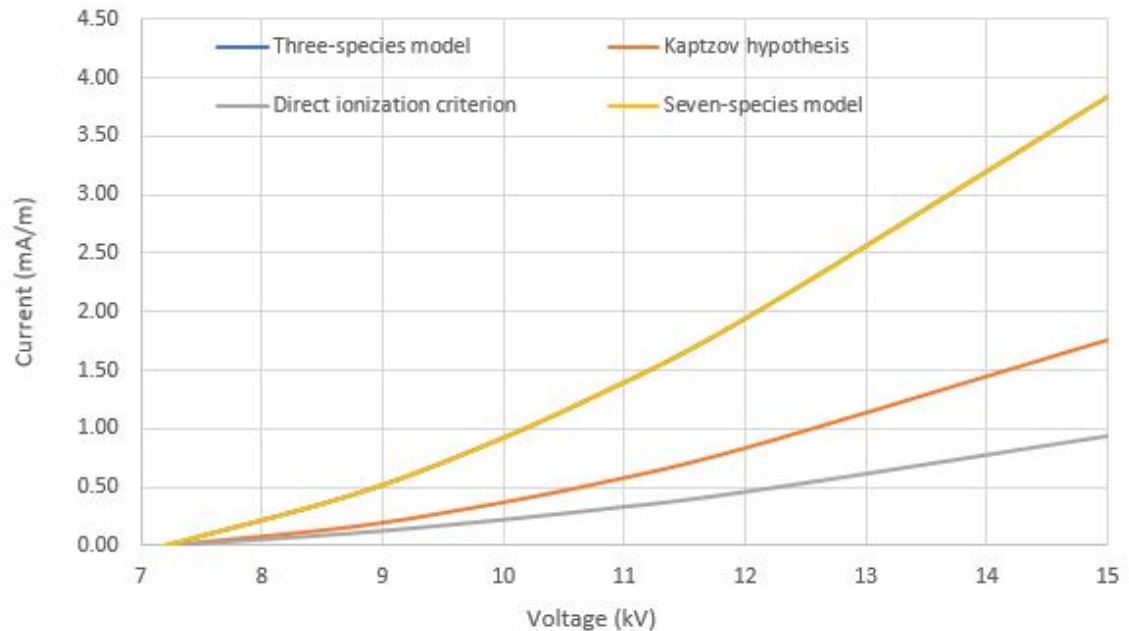
Figure 4-7: V-I curve for the four investigated models

4.7   Conclusions

The negative corona discharge in a wire-cylinder configuration in air has been numerically investigated in this Chapter. The equations of interest were the drift-diffusion equations for the ionic species and the Poisson equation for the electric field. The investigated models included single ionic species, three ionic species and seven ionic species. Monopolar model neglected the ionization layer. Kaptzov hypothesis based on Peek's value and the direct ionization criterion were investigated in this case. The three-species model included the electrons, negative ions O_2^- and positive ions O_2^+. In this case, an iterative algorithm was used and it was necessary to apply an under-relaxation technique in order to have a stable algorithm. The seven-species model included four more ionic species: atomic oxygen O, negative ion of atomic oxygen O⁻, ozone O_3 and the excited species $O_2(^1\nabla g)$. The voltage-current characteristic curve was plotted for each investigated model. In addition, Kaptzov's hypothesis was validated in each case. The spatial distributions of the different ionic species were shown for different voltage levels. The corona current resulting from the three-species model closely agreed with that resulting from the seven-species model. On the other side, a significant difference of the current was reported between the monopolar and multipolar models.

The electric field at the corona electrode surface for all models had practically the same value as Peek's one at the onset voltage. The electric field increased significantly for higher voltages for the model based on the direct-ionization criterion, where the maximum difference was about 43.56%.

Chapter 5

5   Electrohydrodynamic Flow

The electrohydrodynamic flow produced by the electric corona discharge in atmospheric air has been numerically investigated in a needle to plane configuration. Commercial software, COMSOL, has been used to find the solution of the Poisson's equation, the three-ionic drift- diffusion equations and Navier-Stokes equation. These equations predict the distributions of electric potential, space charge density and airflow after calculating the volume force. The volume force is the electric Coulomb force, which is the main factor leading to the EHD flow.

5.1   Model Description

5.1.1   Geometry

The investigated model consists of two electrodes. The first electrode is a grounded large metal plate and the second electrode is a sharp needle, perpendicular to the ground electrode and supplied with a high DC negative potential. The needle has a shape of a cylinder ended with a hemisphere. The needle tip radius is 500 μm, the needle body is 5 cm long and the distance between the ground electrode and the tip of the needle is 2 cm. A two-dimensional axisymmetric model is assumed.

5.1.2   Discretization

A non-uniform distribution of the electric field in the area close to the corona wire is a critical problem for modeling the corona discharge phenomenon. COMSOL, the software used for simulating the problem, is based on the Finite Element Method. A very fine discretization needs to be used in the area of high field gradient in order to achieve an accurate solution. The mesh should also have a non-uniform distribution; very fine triangular elements are formed near the electrode tip and the size of the elements increases gradually going away from the needle tip, where the electric field changes less dramatically. An illustration of the implemented mesh is shown in Figure 5-1.
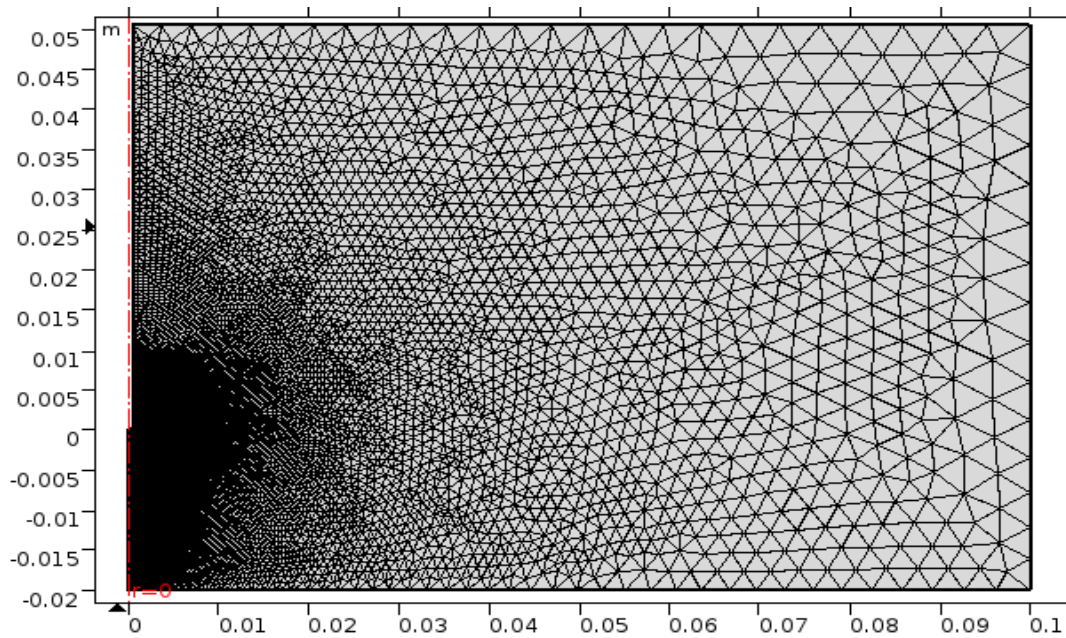
a) Discretization of the whole domain
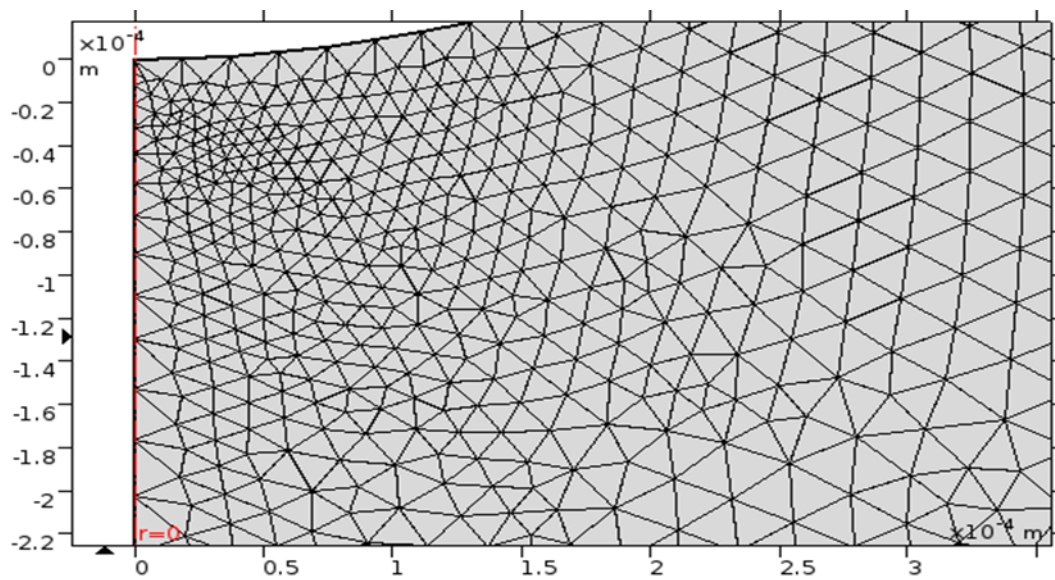
b) Discretization of the domain near the corona tip

Figure 5-1: Discretization of the computational domain

The computational domain is of 0.1 meters long and 0.0705 meters high. The total number of elements is 25,666. A quadratic interpolation is used to approximate the electric field and a linear interpolation for the ionic species concentration. As a result, the model has 89831 degrees of freedom.

5.1.3 Corona and Flow Model

The simulation algorithm for the corona discharge was discussed in Chapters 3 and 4. Three ionic species have been considered in this model: electrons, positive ions and negative ions. The calculation of the space charge density and the electric field is essential before simulating the EHD flow, because the Coulomb force is generated by the action of the electric field on the space charge. For the flow model, a laminar flow has been assumed.

5.2 Simulation Results

For the investigated model Peek's value is 7.9 MV/m, which corresponds the onset voltage of -6 kV. Because a stationary case was investigated, the voltage-current characteristics was calculated for the voltages ranging from -6kV to -12 kV. Moreover, the electron and ionic species concentrations, electric field distributions, maximum and minimum velocities for different voltages have been determined.

The voltage-current characteristics is shown in Figure 5-2. The corona current is initiated when the voltage is above the onset voltage, and it changes as a square function of the applied voltage.
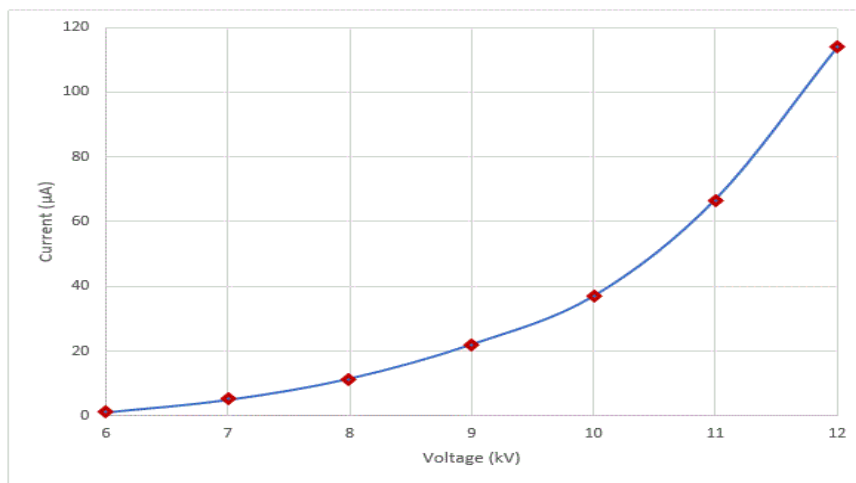
Figure 5-2: V-I characteristic curve

Kaptzov's hypothesis has also been validated in this case. Figure 5-3 shows the value of the electric field on the electrode tip. The electric field is very close to Peek's value at the onset voltage. However, when the supplied voltage increases, the difference between the actual electric field and Peek's value increases.
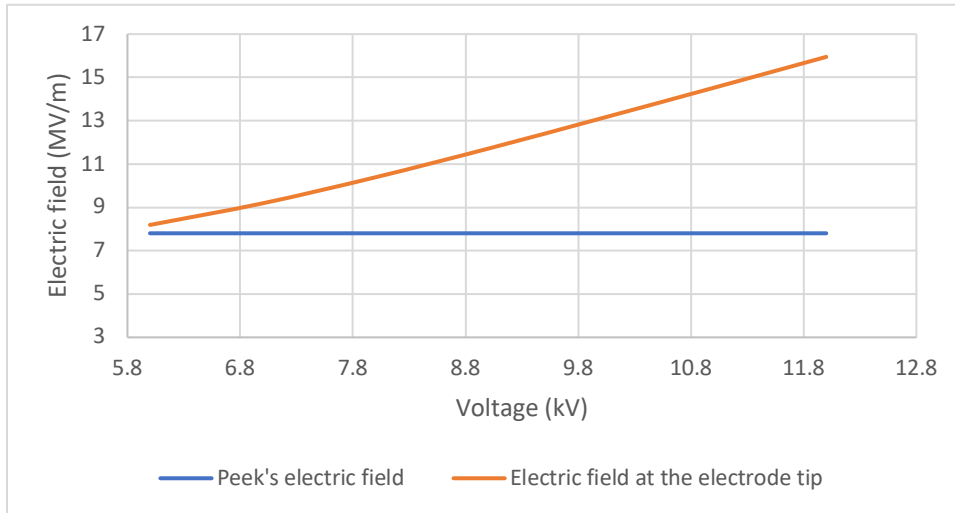
Figure 5-3: Validation of Peek's formula in point-plane configuration

Moreover, comparing the distribution of the electric field along the needle surface with the Peek's value can give some information about the extent of the ionization area. Figure 5-4 shows the electric field in the area near the needle surface at two voltage levels -8 kV and -12 kV. A close in look to the plots implies that the thickness of the ionization area is about 0.2 mm.
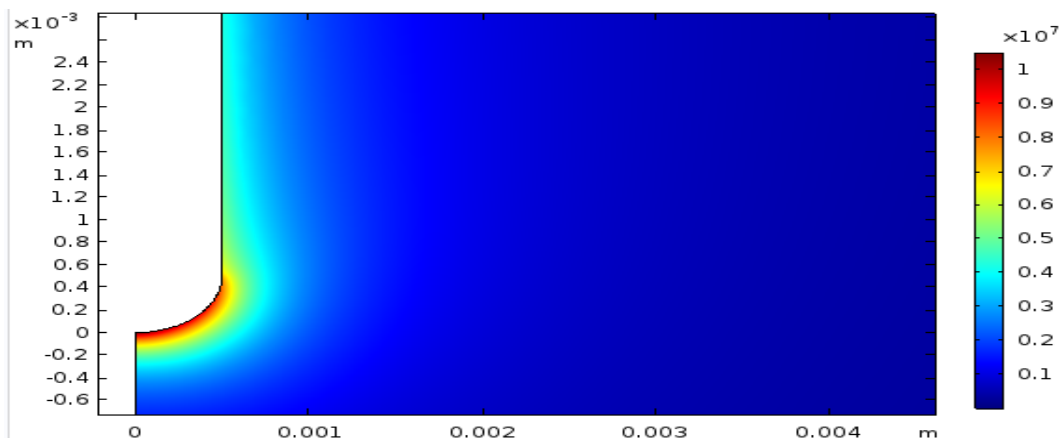
a) Electric field near the needle surface at -8 kV
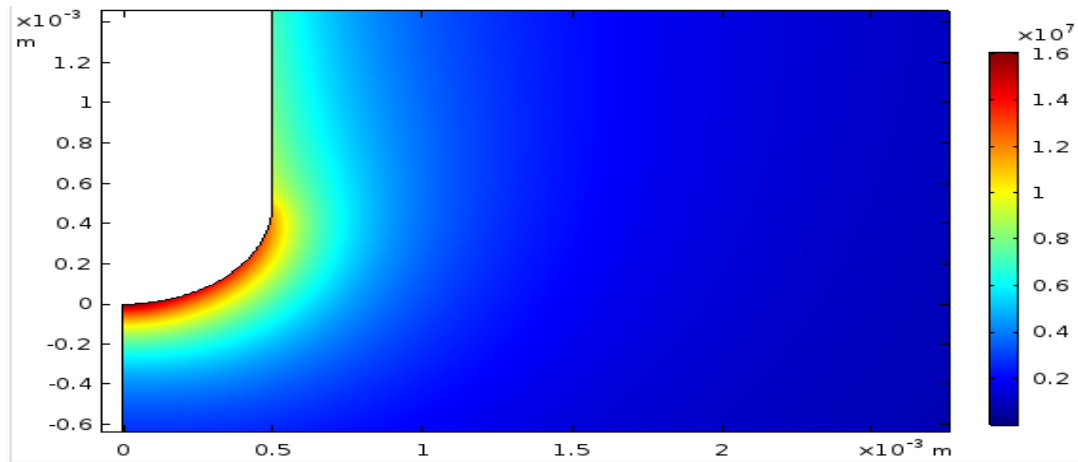
b) Electric field near the needle surface at -12 kV

Figure 5-4: Electric field distribution near the needle surface

The distribution of the three-ionic species has been investigated in the area near the corona electrode. The results for two voltage levels -8kV and -12kV are presented in Figure 5-5.
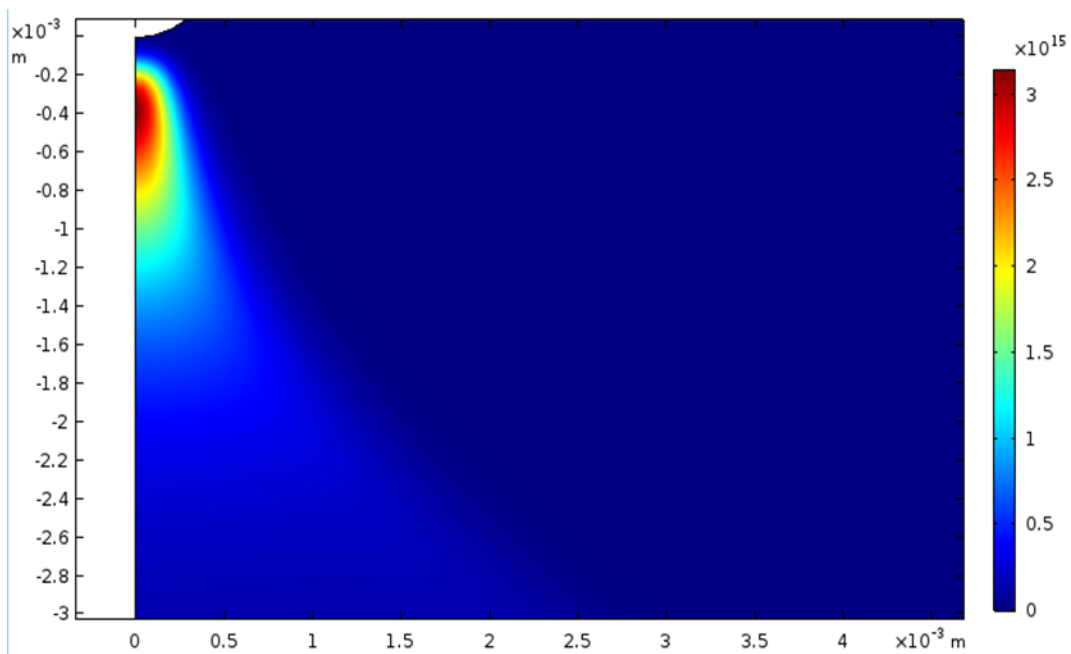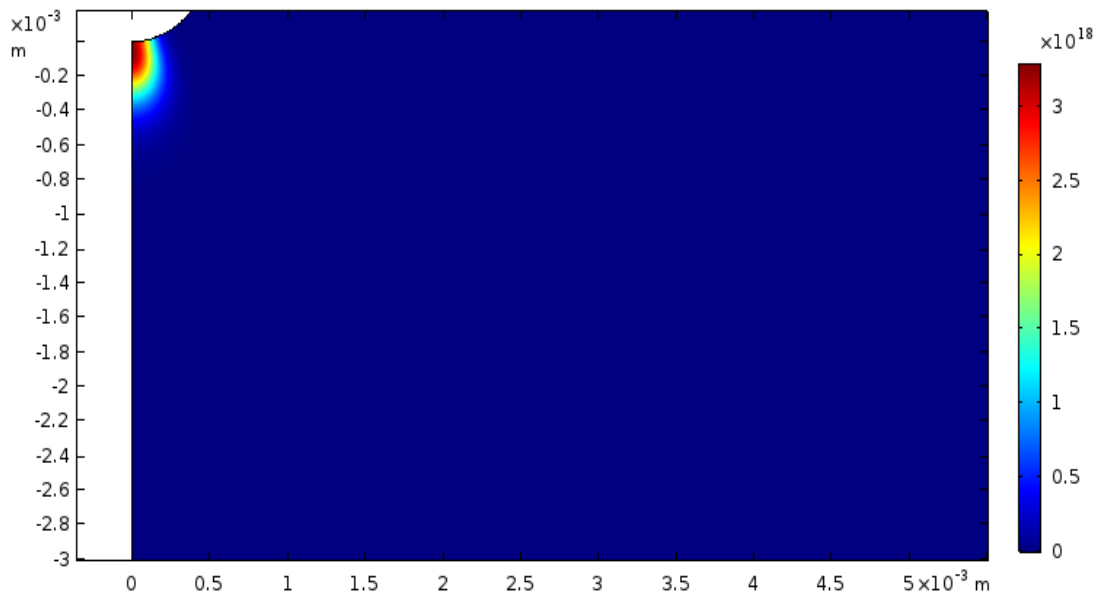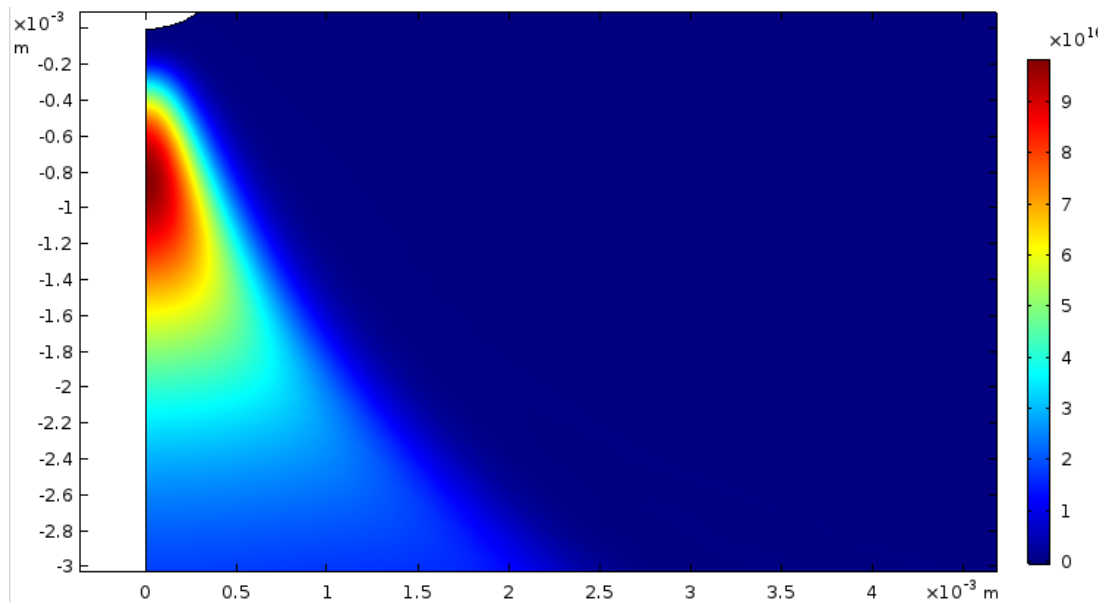
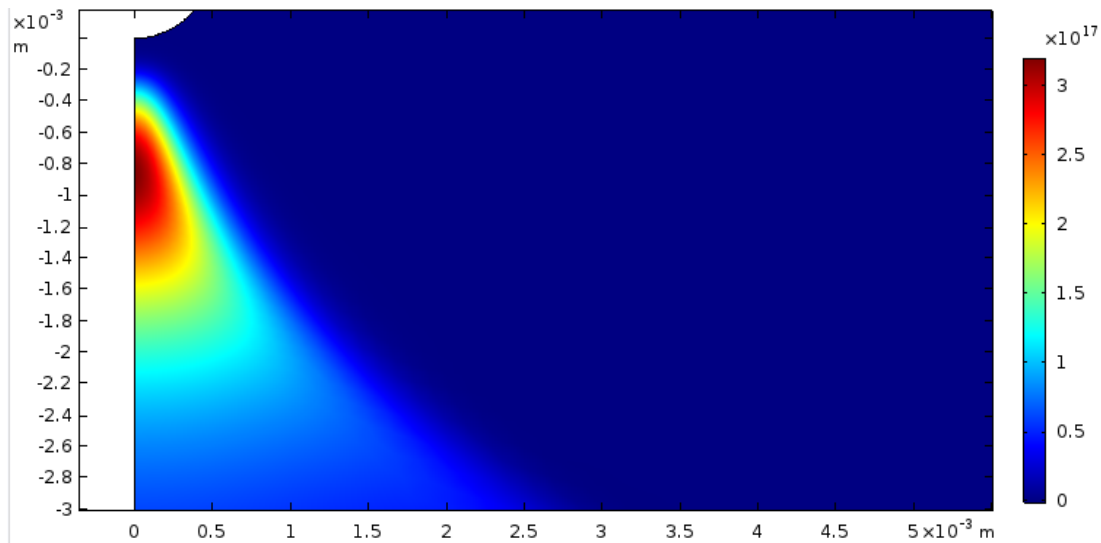a) electron distribution for -8 kV
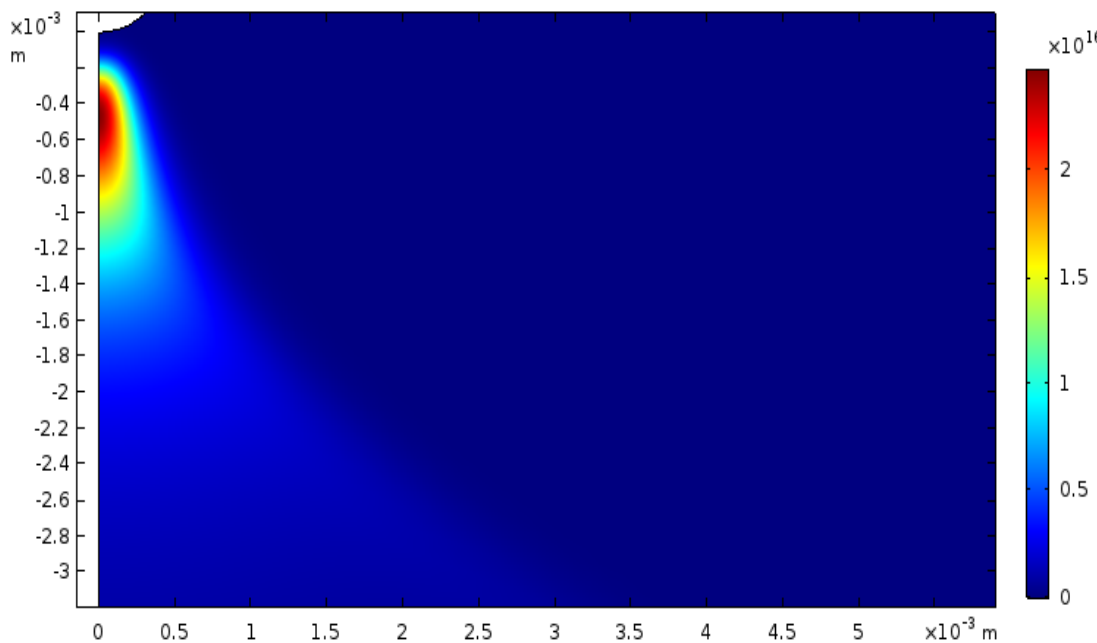
b) electron distribution for -12 kV
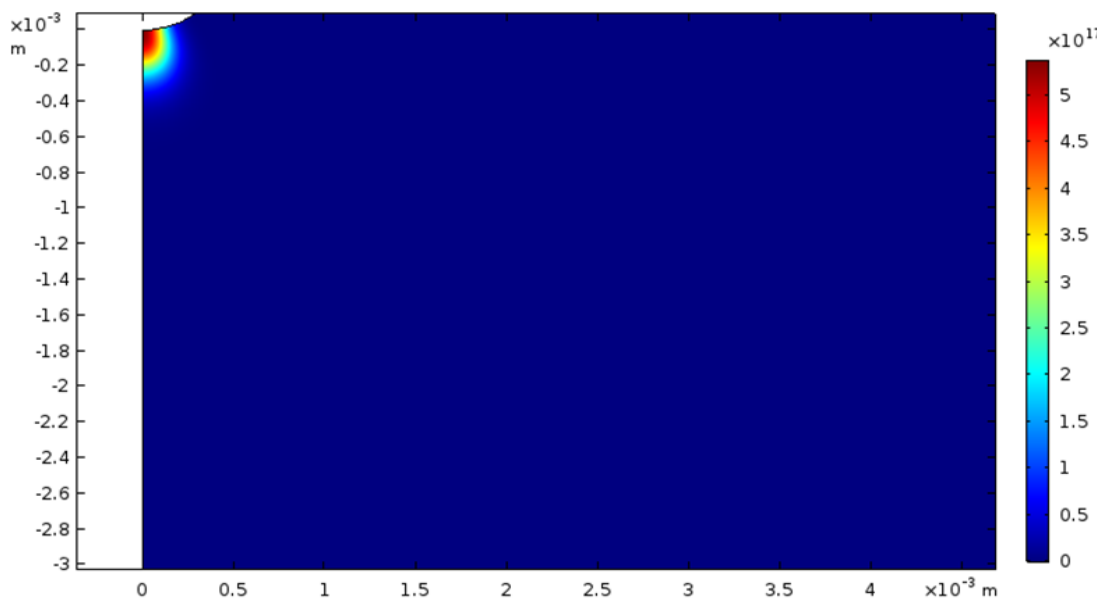
c) positive ions distribution for -8 kV

d) positive ions distribution for -12 kV

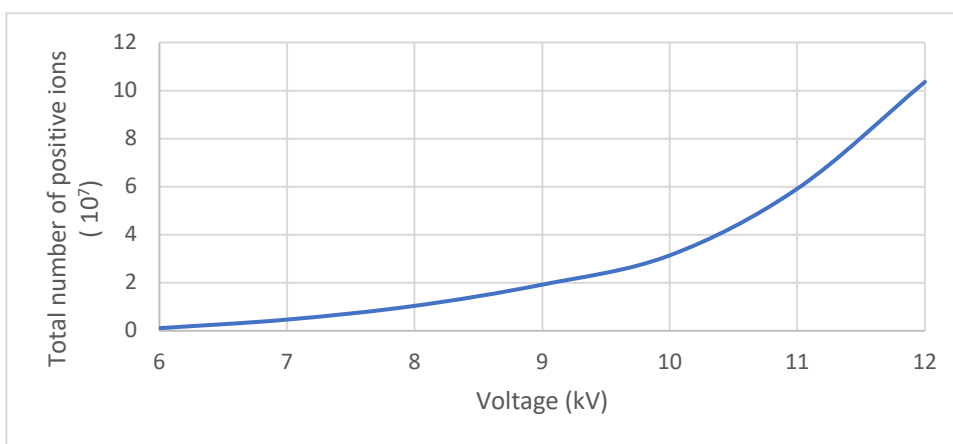e) negative ions distribution for -8kV

f) negative ions distribution for -12 kV

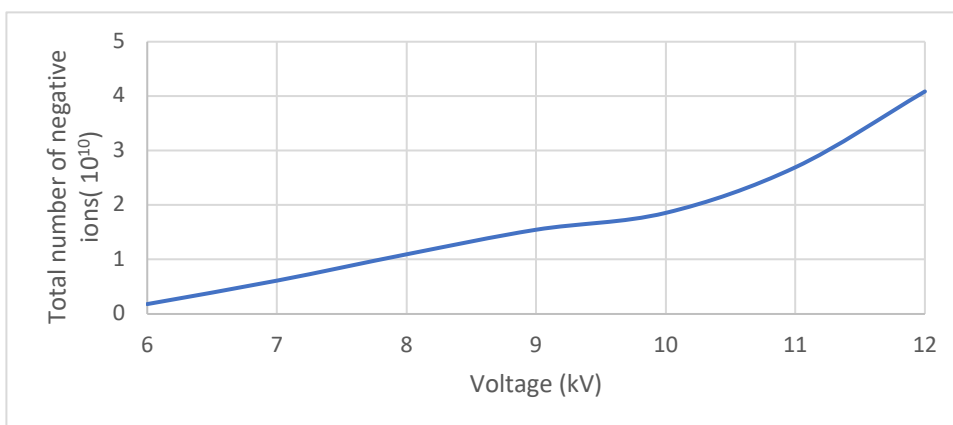**Figure 5-5: Distribution of all ionic species in the air gap for voltages -8 kV and -12kV**

Since the voltage applied to the corona electrode is negative, it is logical to observe the migration of negative ions away from the corona electrode, and the attraction of positive ions towards the corona electrode. For the electron distribution, this density near the discharge electrode is small because the electrons are produced by secondary emission. However, the electron concentration increases due to the avalanche ionization, and the maximum number of electrons can be observed near the edge of the ionization layer. Moreover, the total number of electrons and positive ions increases as a approximately square function of voltage, what is shown in Figure 5-6. On the other hand, the total number of negative ions increases approximately linearly with voltage for voltages smaller than 9 kV; this changes to approximately square dependence for higher voltages.
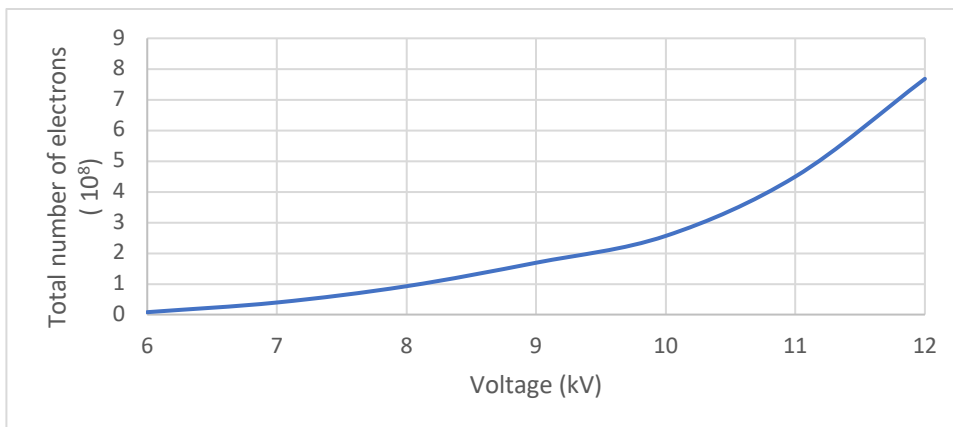
a) Total number of electrons

b) Total number of positive ions

c) Total number of negative ions

Figure 5-6: Variation of number of different ionic species with voltage

5.3   Simulation Results of EHD Flow

Figure 5-7 shows the distribution of the magnitude of the EHD force near the needle tip
for the voltage levels of -8 kV and -12 kV. The force has a maximum value at the needle
tip. It starts decreasing going away from the tip in both r-direction and z-direction.
Regarding the direction of the EHD force, the concentration of positive ions is higher
than that of the negative ions inside the ionization region. As such, the total charge is
positive which implies that the force is directed towards the needle electrode. In the drift
zone the net charge is negative, so the Coulomb force is directed towards the ground
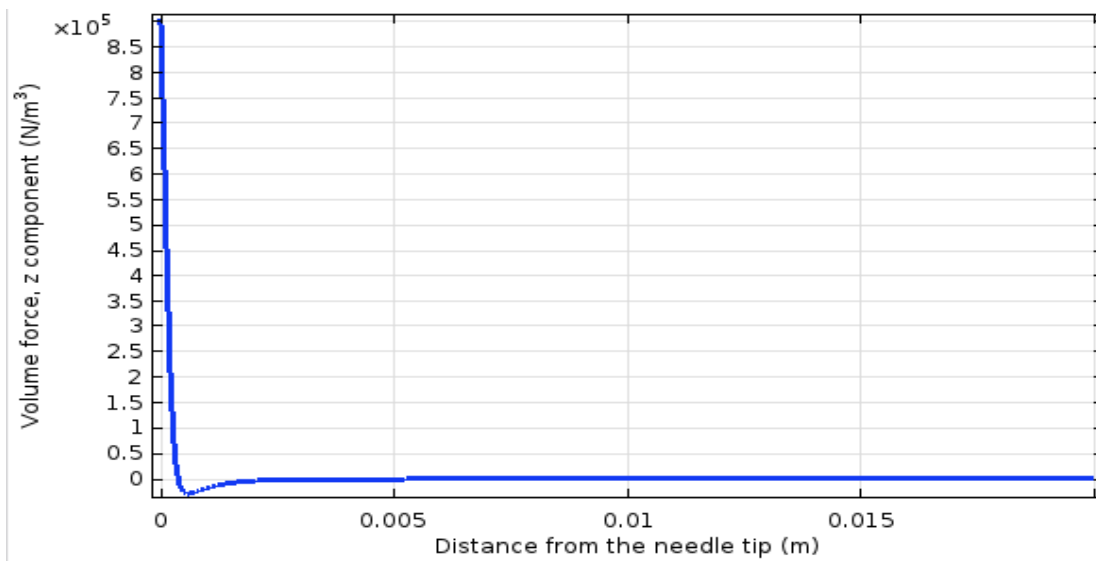electrode.
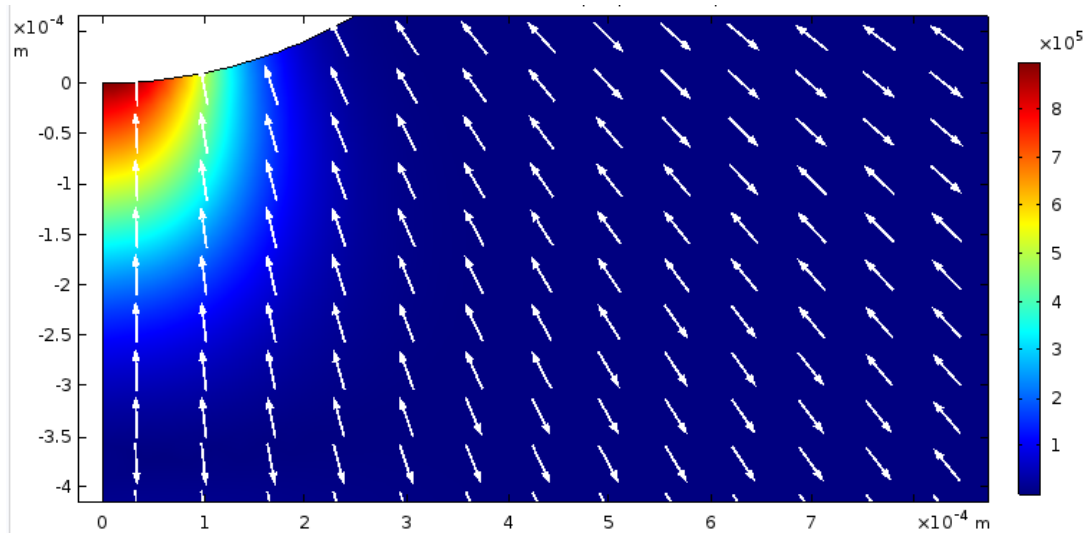
a)   Spatial distribution of body force at -8 kV
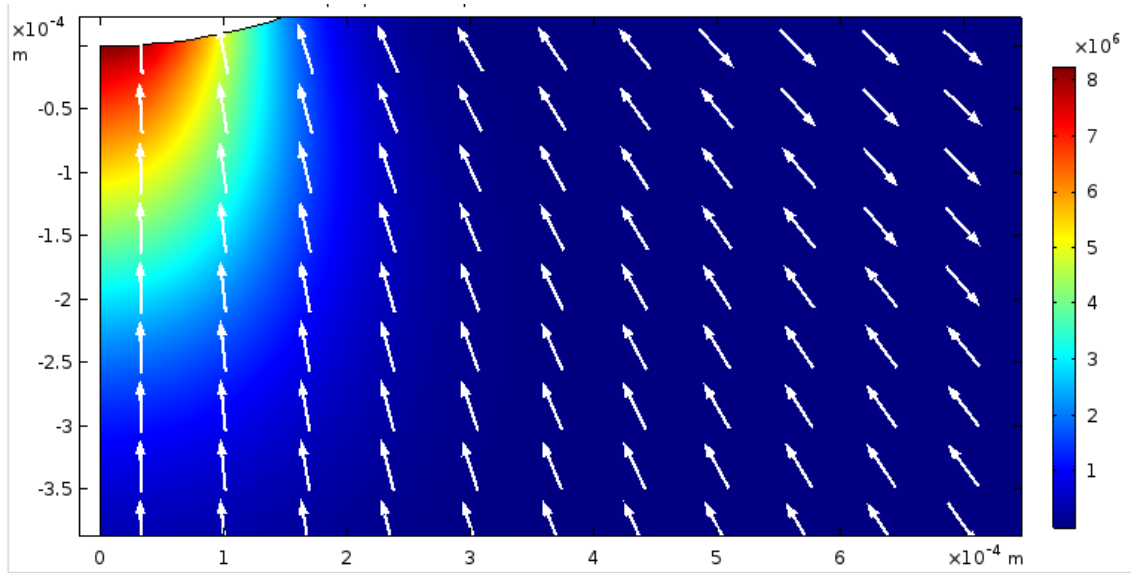
b) Spatial distribution of body force at -12 kV

Figure 5-7: Spatial distribution of body force near the needle tip

Figure 5-8 shows the distribution of the EHD force in the z direction along the axis of symmetry for the two voltage levels: -8 kV and -12 kV. It is interesting to see the change in the direction of the EHD force near the corona needle tip. The behavior of the curve implies that the flow pattern is more complicated than it was previously reported in literature.

a) Axial component of the EHD body force for -8 kV
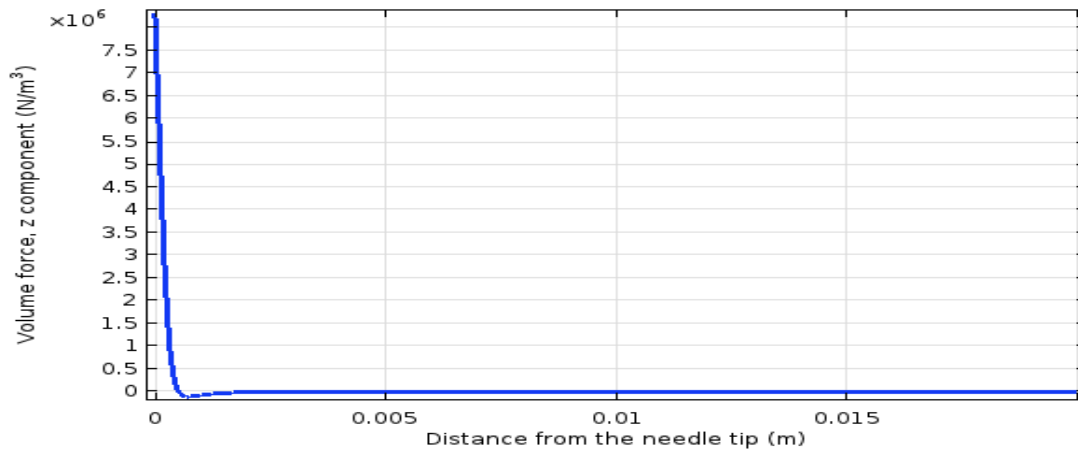

b) Axial component of the EHD body force for -12 kV

Figure 5-8: Axial component of the EHD body force along the axis of symmetry

Figure 5-9 shows flow streamlines in the whole airgap between both electrodes for the applied voltage of -8kV and -12 kV. In addition to a dominant vortex occupying most of the airgap, an additional vortex, much smaller than the first one, appears in the area close to the corona electrode tip. This small vortex has a small size of approximately 0.5x0.5mm; perhaps this is why it has not been observed experimentally.
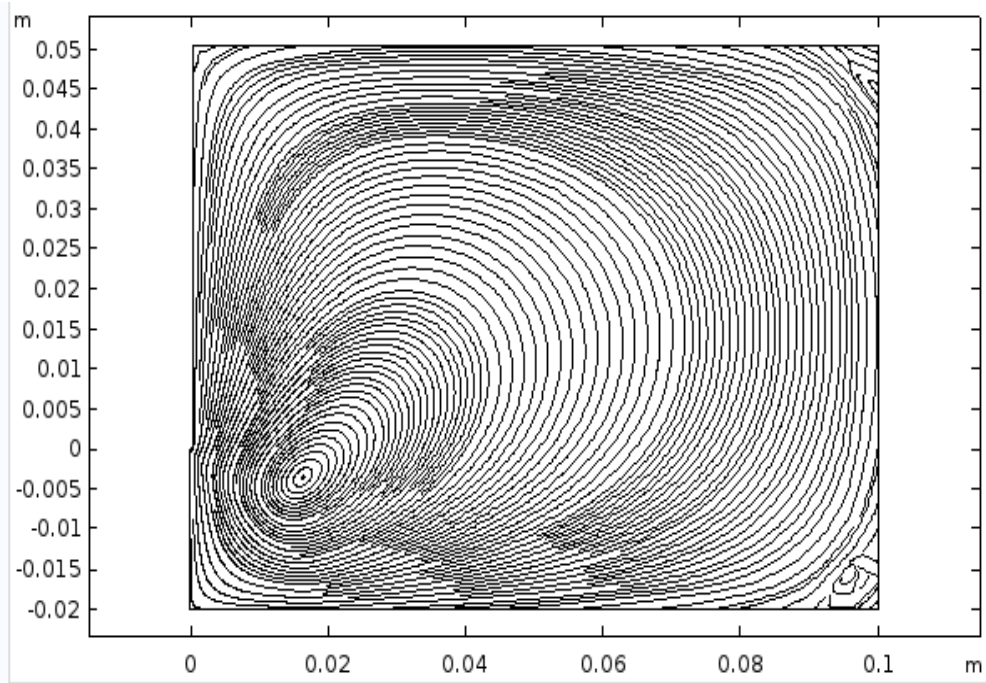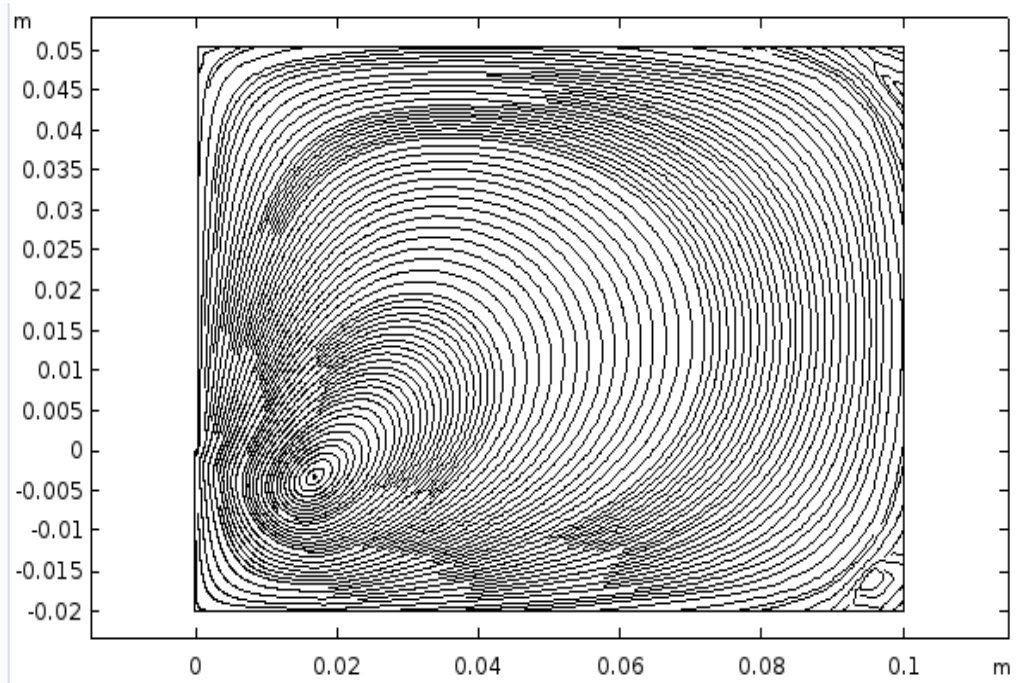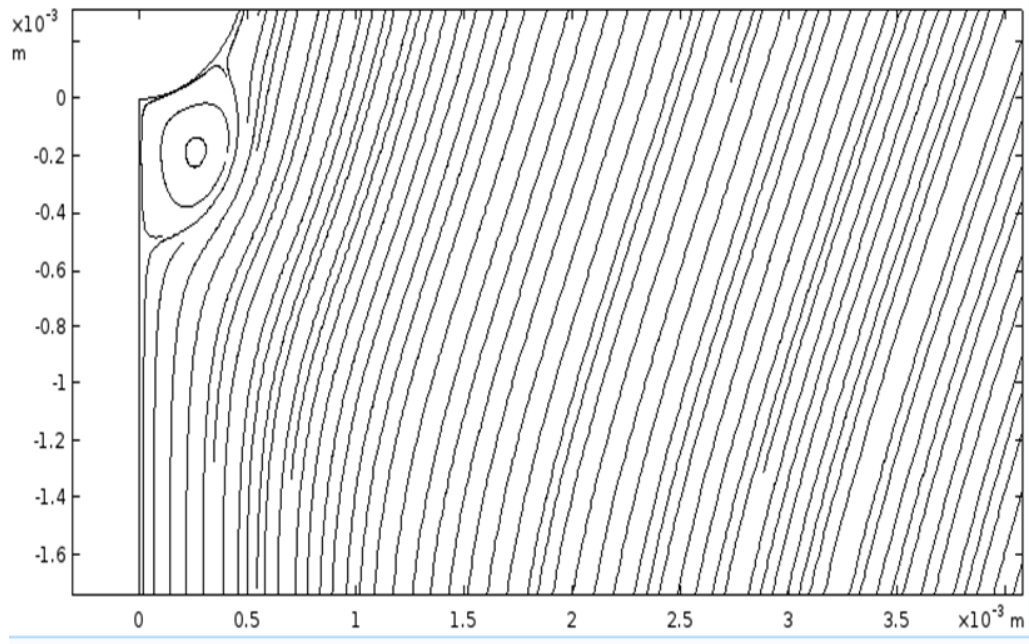
a) Streamlines at -8 kV
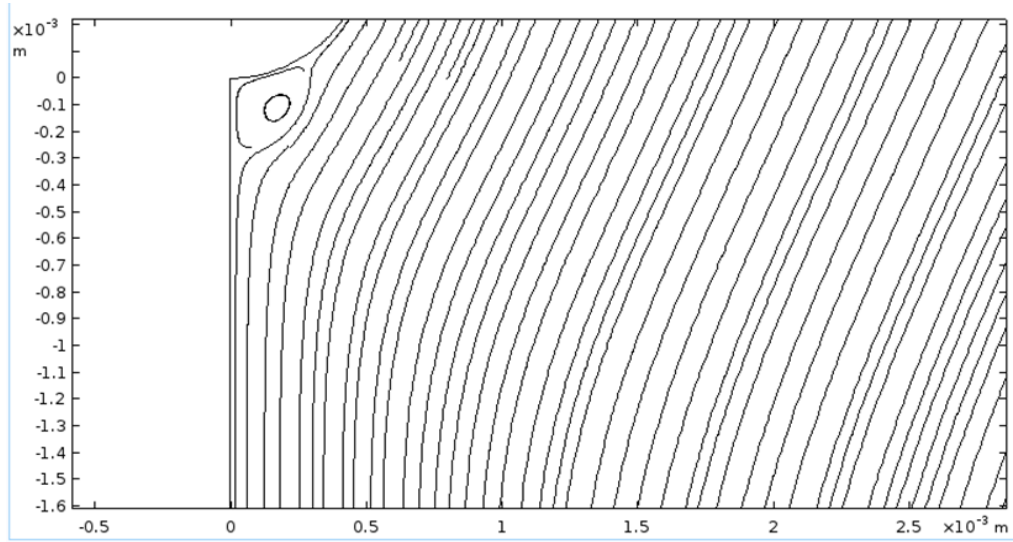
b) Streamlines at -8 kV near the needle tip

c) Streamlines at -12 kV

d) Streamlines at -12 kV near the discharge tip

Figure 5-9: Velocity streamlines for airflow

Figure 5-10 shows the airflow velocity magnitude when the applied voltage is -8 kV and -12 kV. Two local velocity maxima can be observed in an area between both electrodes. Near the corona electrode, the velocity is directed towards the discharge electrode and the point of the maximum velocity is about 0.14 mm away from the electrode tip. The second point of maximum is about 1.6 mm from the electrode tip and at that point the velocity is directed towards the ground electrode. The velocity magnitude strongly increases with the increasing voltage.
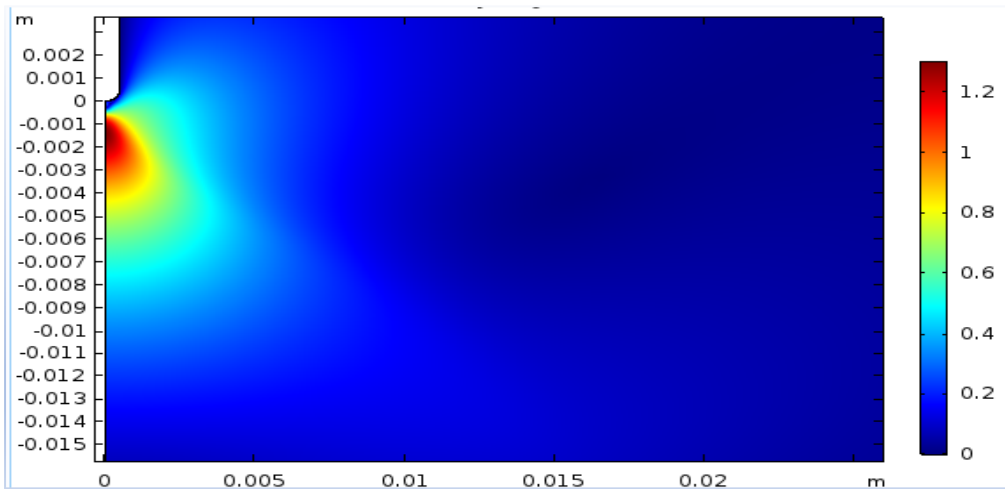
a) Velocity magnitude at -8 kV
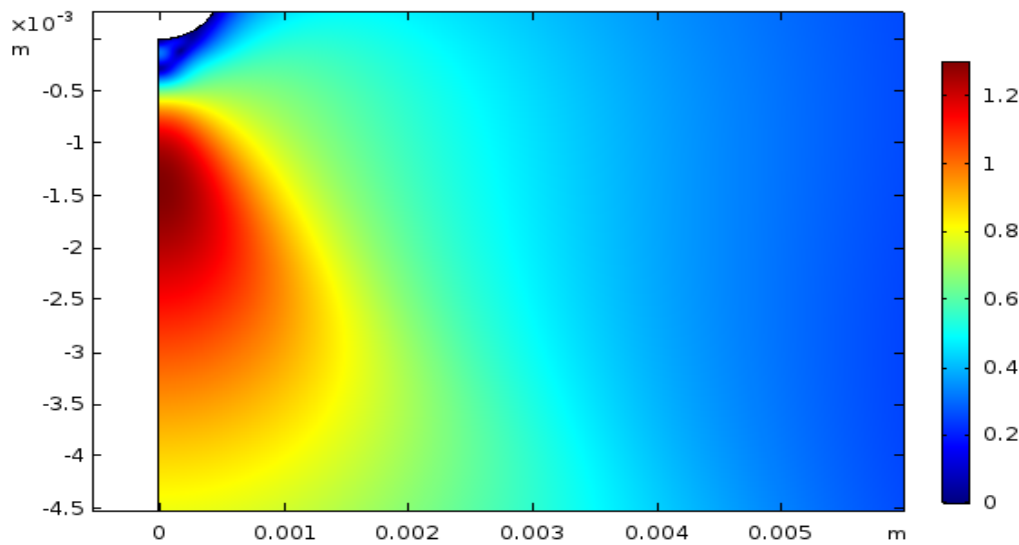
b) Velocity magnitude near the corona electrode at -8 kV
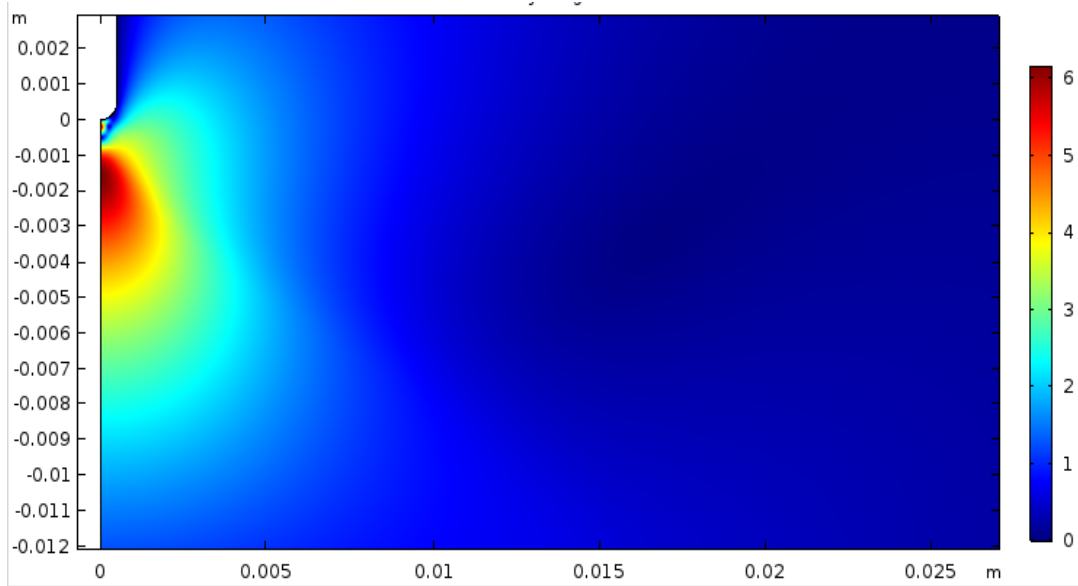
c) Velocity magnitude in the whole domain at -12 kV
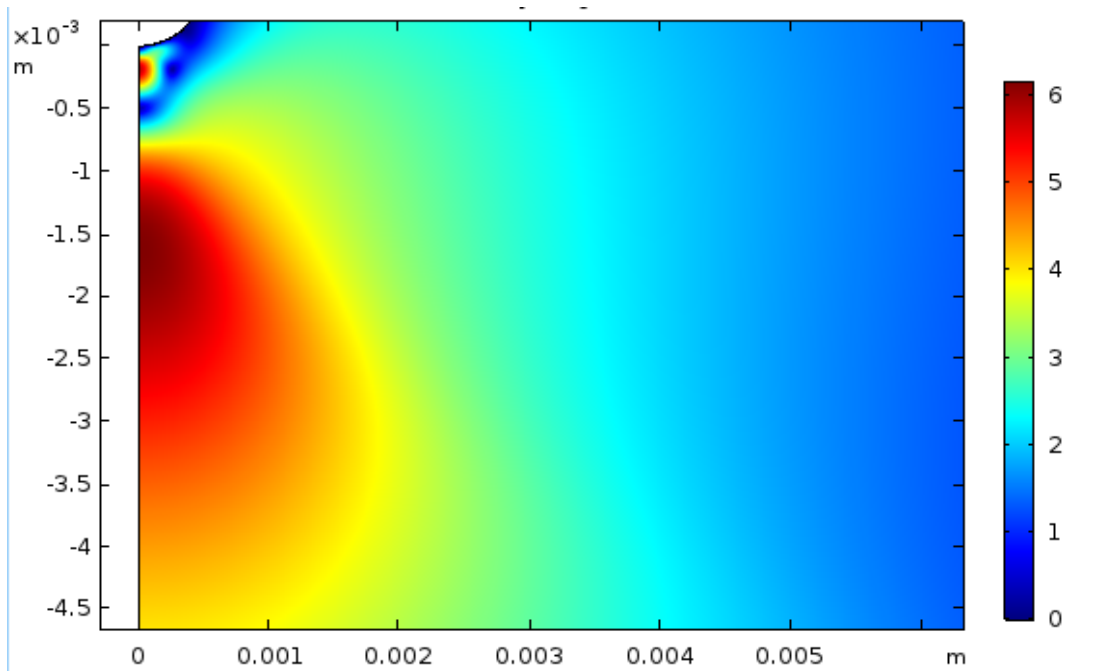
d) Velocity magnitude near the corona electrode at -12 kV

Figure 5-10: Velocity magnitude of the airflow at -8 kV and -12 kV (m/s)

On the other hand, the radial and axial flow velocity for voltage level -12 kV in the whole airgap and near the needle tip is shown in Figure 5-11.
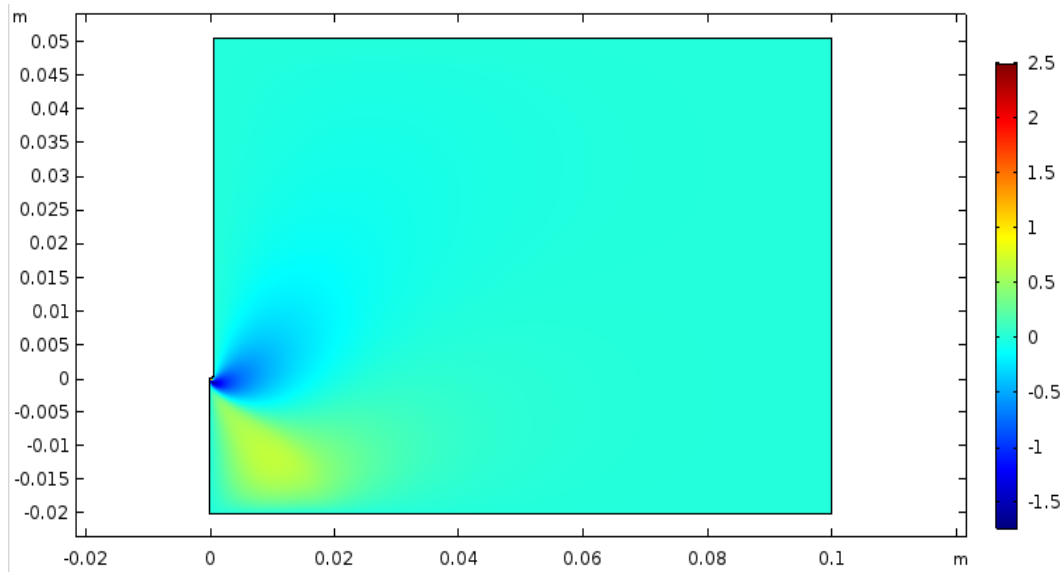
a) Radial velocity at – 12 kV
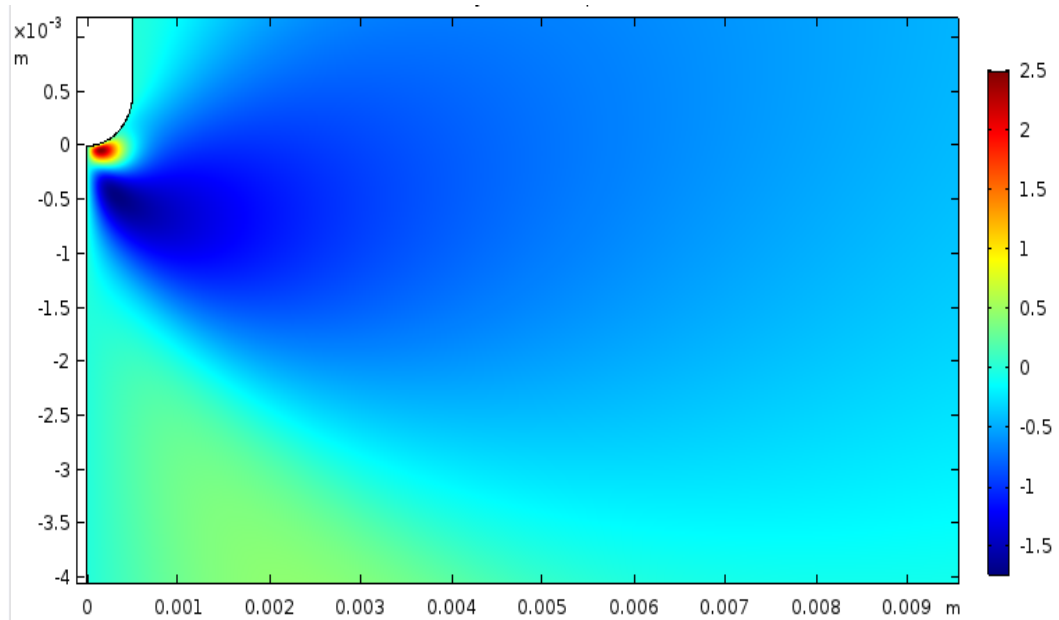
b) Radial velocity near the needle tip at -12 kV
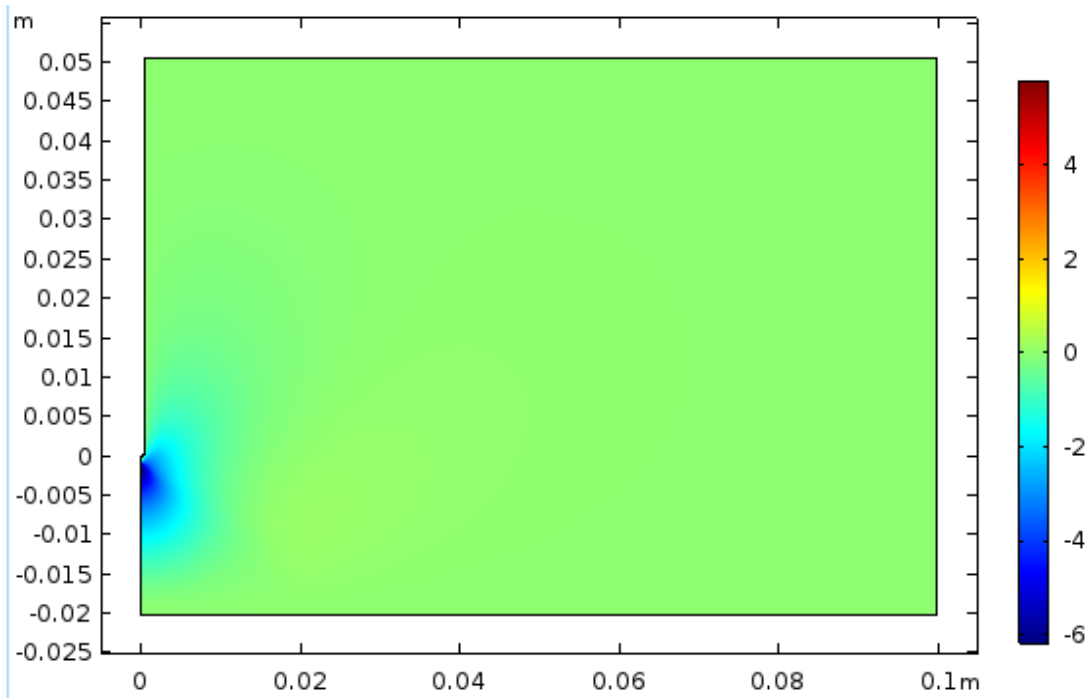
c) Axial velocity at -12 kV
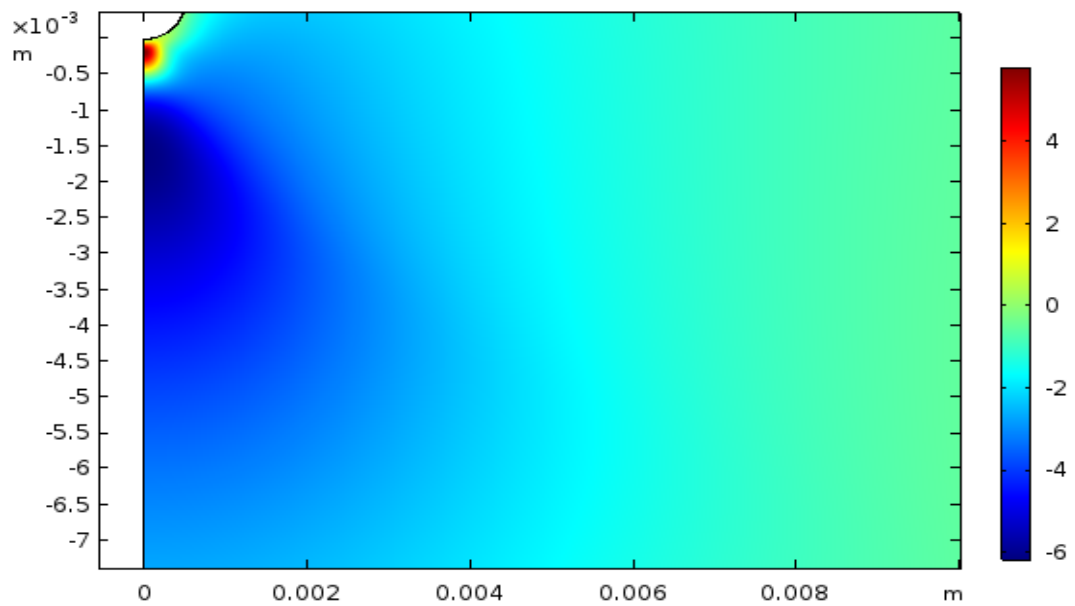
d) Axial velocity near the needle tip at -12 kV

Figure 5-11: Axial flow velocity (m/s)

The axial flow velocities on the symmetry axis for different supply voltages are shown in Figure 5-12. It is obvious that higher voltages cause higher maximum and lower minimum axial velocities. This can be attributed to the higher Coulomb force resulting from the higher electric field and space charge density. It can also be noticed that the maximum and minimum velocities take place at the same two points for all voltage levels. At the corona electrode, the velocity is equal to zero due to non-slip boundary conditions, and then it increases dramatically to a positive value at some point near the corona electrode. After this point, the axial velocity changes from positive to negative values which is associated with the change of the Coulomb force direction. The axial velocity starts increasing again until it reaches zero at the collecting electrode.
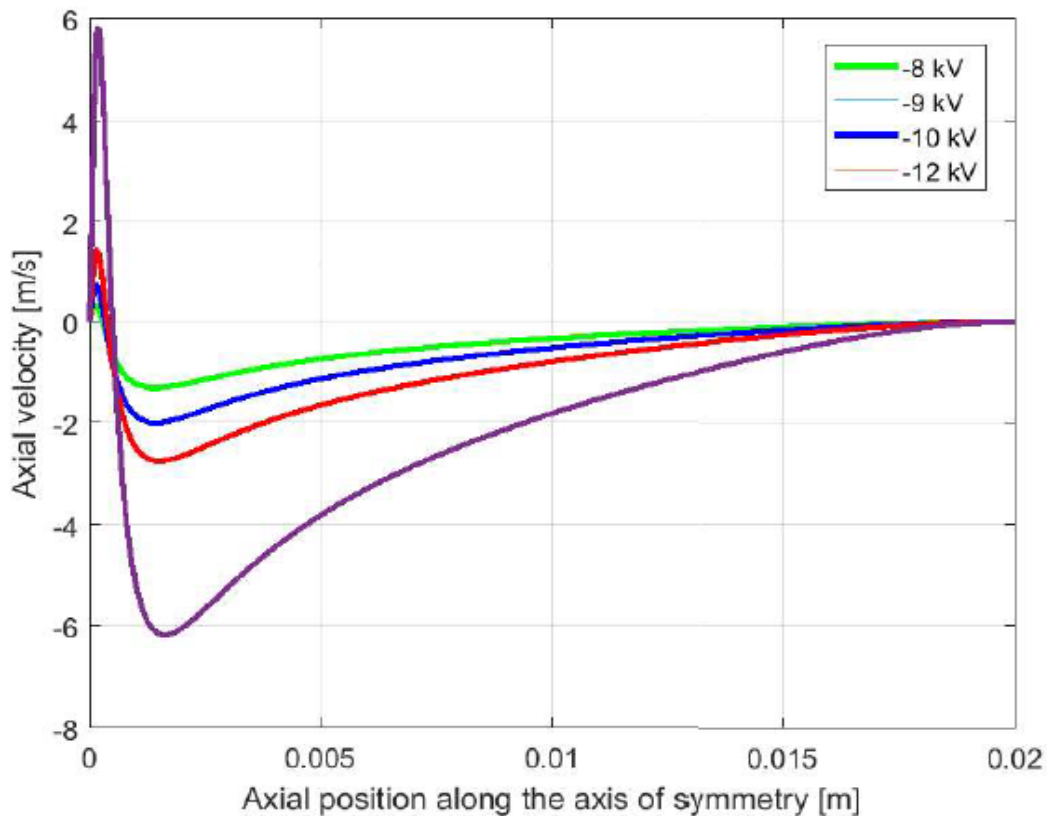
Figure 5-12: Axial velocity along axis of symmetry for different voltage levels

Figure 5-13 shows that the minimum and maximum velocity curves behave differently with the increasing voltage. The maximum velocity increases very slightly until -8 kV from which it starts increasing until it reaches 5.8 m/s at the voltage equal to -12 kV. The

minimum velocity decreases uniformly starting from the onset voltage until it reaches -6.17 m/s at the voltage level -12 kV.
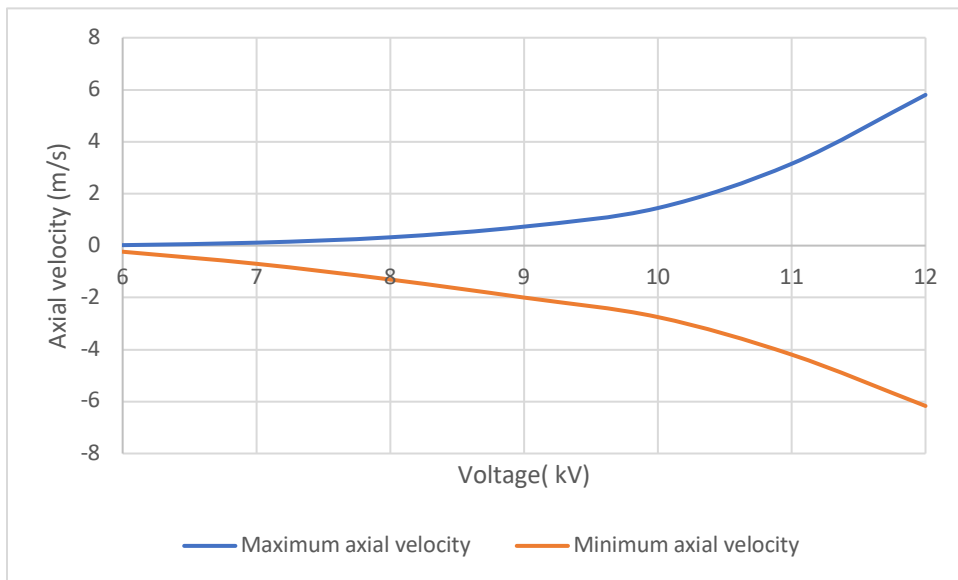
Figure 5-13: Maximum and minimum axial velocities for different voltage levels

Figure 5-14 presents the distribution of pressure in the air gap for two voltage levels: -8 kV and -12 kV in the area near the corona electrode. The maximum pressure increases dramatically as the applied voltage to the corona electrode increases. The pressure is high near the corona tip.
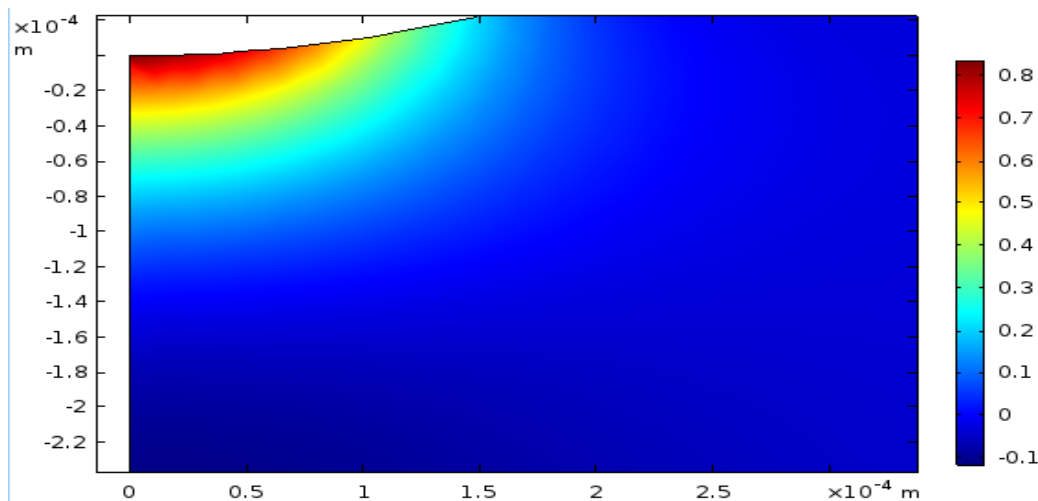
a) Pressure distribution near corona electrode at -8 kV
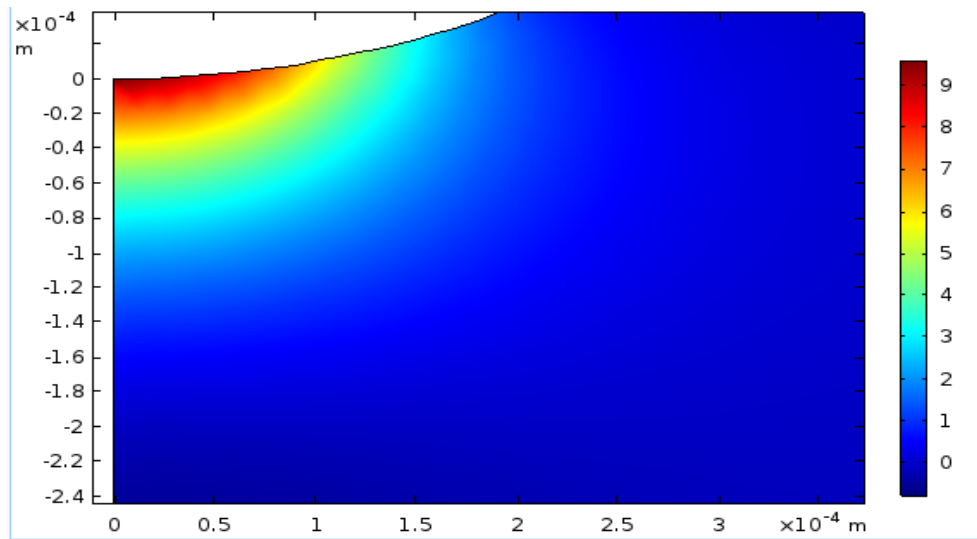
b) Pressure near the corona electrode at -12 kV

Figure 5-14: Pressure near the corona tip (Pa)

5.4   Conclusions

The previous studies of EHD flow never considered a very thin ionization layer near the discharge electrode. In this Chapter, EHD flow in air produced by negative corona discharge in a needle- plate configuration has been investigated, with a special attention to this region.

As the EHD flow is caused by the Coulomb force, the electrical parameters of the problem must be determined first. This was done assuming a stationary discharge model, which included three ionic species (electrons, positive and negative ions) and five ionic reactions. The voltage-current characteristics and distribution of all ionic species have been determined.

The simulation results predict a small flow vortex near the corona electrode, where flow is directed towards the discharge electrode. The velocity preserves the same pattern for different applied voltage levels, but the velocity magnitude increases with the voltage level. Spatial distributions of the velocity magnitude, pressure and streamlines have also been presented.

Chapter 6

6   Conclusions

The first section in this Chapter summarizes all results of the numerical simulations presented in this thesis. The second section describes the unsuccessful attempts to add sub-routines to replace some built-in functions in COMSOL and to investigate other discharge models.

6.1   Summary of the Thesis

Simplified numerical models to simulate negative corona discharge and EHD flow are presented in this thesis. The studied models included single-species, three-species and seven-species in 1D axisymmetric wire-cylinder and 2D point-plane configurations. The following conclusions summarizing the obtained results can be formulated:

•   For the unipolar corona discharge model, Kaptzov's hypothesis is compared with the model using the direct ionization criterion. The current-voltage characteristics obtained from both models are practically the same. The three-species and seven-species models also yield the same discharge characteristics. However, the difference in the discharge current between the monopolar and multipolar models is quite noticeable and it increases as the voltage level increases.

•   The unipolar models based on Kaptzov's hypothesis and direct ionization criterion predict a very similar value of the electric field on the corona wire surface at the discharge onset. In the model based on Kaptzov's hypothesis the electric field remains practically constant, if a small numerical error is neglected, for all voltage levels. In the case of direct ionization criterion, the electric field increases as the voltage increases and the maximum difference is about 44% when compared to Peek's value. The electric field magnitude at the corona wire obtained from the seven-species model is practically the same as that resulting from the three-species model. Both multipolar models predict that the electric field agrees quite closely with Peek's value.

•   A 2D axisymmetric needle-plate configuration has been studied in this thesis using three ionic species to predict the EHD flow pattern. The results predict a double vortex pattern: major one occupying the majority of the air gap and another, much smaller, localized near the discharge point. This pattern corresponds to the direction of the body force, which is directed towards the discharge point in the ionization layer, where the net electric charge is positive, and towards the ground plate in the drift zone. This pattern has never been reported before.

6.2   Unsuccessful Attempts with Corona Simulation

The most important limitation of COMSOL software is its inability to properly handle drift-diffusion equations governing the ionic charge transport. This parabolic equation is dominated by the first derivative of the unknown space charge density distribution. The conventional techniques are not very accurate in this case and are often divergent, or produce unphysical oscillations. One way to handle this problem is to use very fine domain discretization, but this leads to very time-consuming calculations, or to introduce an artificial diffusion, which obviously distorts the results. A better way to handle this problem is to use some special techniques, for example Flux Corrected Transport [21] or Total Variation Diminishing [72]. The idea attempted in this thesis was to run COMSOL from MATLAB and replace the software solver with separately written computer code. Specifically, the plan was to substitute the stiffness matrix created in COMSOL by a user-built matrix, written as a MATLAB function, determined using the Total Variation Diminishing technique. After spending some time on this project and contacting COMSOL support team, it became clear that this idea would require a detailed knowledge of the COMSOL data structures. Unfortunately, this information is confidential and COMSOL staff refused to cooperate on this.

Another project that was initiated, but without successful completion, was the numerical simulation of Trichel pulses in a 1D wire-cylinder configuration using three, and possible a higher number, ionic species. The goal was to check how the electric field on the corona electrode surface compares with Peek's value. Unfortunately, the pulse train couldn't be reproduced. One pulse was observed, but everything seemed to fade away with time. This may be a more general problem, as corona discharge is never truly 1D

phenomenon. Even for infinitely long wire the discharge has a form of concentrated tufts, which makes the problem 3D. Actually, nobody so far was able to reproduce Trichel pulses in 1D case.

References

1. J.A. Cross, Electrostatics. CRC Press, 1987.

2. M. Goldman, A. Goldman and R. Sigmond, "The corona discharge, its properties and specific uses", Pure and Applied Chemistry, vol. 57, no. 9, 1985.

3. J. Chang, P. Lawless and T. Yamamoto, "Corona discharge processes", IEEE Trans. Plasma Sci, vol. 19, no. 6, pp. 1152-1166, 1991.

4. L. Loeb, "Recent Developments in Analysis of the Mechanisms of Positive and Negative Coronas in Air", J. of Appl. Phys., vol. 19, no. 10, pp. 882-897, 1948.

5. M. Robinson, "A history of the electric wind", J. of Phys. 30 366–72, 1962.

6. A. Chattock, "On the velocity and mass of the ions in the electric wind in air", The London, Edinburgh, and Dublin Philosophical Magazine and Journal of Science, vol. 48, no. 294, pp. 401-420, 1899.

7. R. Codina, "Comparison of some finite element methods for solving the diffusion-convection-reaction equation", Comp. meth. app. Mech. Eng. 156(1) 185-210, 1998

8. G.S.P. Castle, "Industrial applications of electrostatics:", J. of Electrostat., vol. 51-52, pp. 1-7, 2001.

9. P. Maruvada, Corona performance of high-voltage transmission lines. Inglaterra: Research Studies, 2000.

10. M. Sakiku, Elements of electromagnetics. Oxford university press, 2014.

11. F. Peek, Dielectric Phenomena in high voltage engineering, McGraw-Hill Book Company, Incorporated, 1929.

12. L. Loeb, Electrical coronas, their basic physical mechanisms. Berkeley: University of California Press, 1965.

13. M. Ogasawara, "Analysis of Formation Stage of Corona Discharge", Journal of the Physical Society of Japan, vol. 21, no. 11, pp. 2360-2372, 1966.

14. M. Sarma and W. Janischewskyj, "Analysis of Corona Losses on DC Transmission Lines Part II - Bipolar Lines", IEEE Trans. Power App. Syst, vol. 88, no. 10, pp. 1476-1491, 1969.

15. N. Malik, "A review of the charge simulation method and its applications", IEEE Elect. Insul. Mag, vol. 24, no. 1, pp. 3-20, 1989.

16. K. Adamiak, "Simulation of corona in wire-duct electrostatic precipitator by means of the boundary element method", IEEE Trans. Ind. Appl., vol. 30, no. 2, pp. 381-386, 1994.

17. J. McDonald, W. Smith, H. Spencer III and L. Sparks, "A mathematical model for calculating electrical conditions in wire- duct electrostatic precipitation devices", Journal of Applied Physics, vol. 48, no. 6, pp. 2231-2243, 1977.

18. W. Janischewskyj and G. Cela, "Finite element solution for electric fields of coronating DC transmission lines", IEEE Trans. Power App. Syst, ,vol.-98 no. 3, pp. 1000-1012, 1979.

19. P. Levin and J. Hoburg, "Donor cell-finite element descriptions of wire-duct precipitator fields, charges, and efficiencies", IEEE Trans. Ind. Appl., vol. 26, no. 4, pp. 662-670, 1990.

20. O. Zienkiewicz and R. Taylor, The finite element method. Oxford: Butterworth-Heinemann, 2000.

21. R. Morrow, "Theory of negative corona in oxygen". Phys. Rev. A 32.3 (1985)

22. J. Jones and M. Davies, "A critique of the Deutsch assumption", Journal of Physics D: Applied Physics, vol. 25, no. 12, pp. 1749-1759, 1992.

23. M. Abdel-Salam, M. Farghally and S. Abdel-Sattar, "Finite element solution of monopolar corona equation", IEEE Elect. Insul. Mag, vol. -18, no. 2, pp. 110-119, 1983.

24. M. Abdel-Salam, M. Farghaly and S. Abdel-Sattar, "Monopolar Corona on Bundle Conductors", IEEE Power Eng. Rev. , vol. -2, no. 10, pp. 59-60, 1982.

25. J. Chen, J. H. Davidson, " Model of the negative DC corona plasma: comparison to the positive DC corona plasma", Plasma chemistry and plasma processing. 2003

26. K. Adamiak, "Simulation of corona in wire-duct electrostatic precipitator by means of the boundary element method", IEEE Trans. Ind. Appl., vol.30, no.2, pp.381-386, 1994.

27. K. Adamiak and P. Atten, "Simulation of corona discharge in point-plane configuration", J. of Electrostat., vol.61, p. 85-98, 2004

28. GE. Georghiou, R. Morrow, AC. Metaxas, "Characterization of point-plane corona in air at radio frequency using a FE-FCT method", J. of Appl. Phys, 1999 Sep 7;32(17):2204.

29. X. Liang, S. Jayaram, A. A. Berezin and J. S. Chang, "Modeling of the electrical parameters of a wire-cylinder electrostatic precipitator under pulse energization", IEEE Trans. Ind. Appl., vol.38, no.l, pp.35-41, 2002.

30. B. S. Rajanikanth and B. R. Prabhakar, "Modeling of prebreakdown VI characteristics of a wire-plate electrostatic precipitator operating under combined dc-pulse energization", IEEE Trans. Dielectr. Electr. Insul. , vol.l, no.6, pp. 1058-1067, Dec. 1994.

31. L. Salasoo and J. K. Nelson, "Simulation and measurement of corona for electrostatic pulse powered precipitators", J. Appl. Phys., vol.58, no.8, pp.2949-2957, 1985

32. J. Zhang and K. Adamiak, "A multi-species DC stationary model for negative corona discharge in oxygen; point-plane configuration", J. of Electrostat., vol. 65, no. 7, pp. 459-464, 2007.

33. K. Yanallah and F. Pontiga, "A semi-analytical stationary model of a point-to-plane corona discharge", Plasma Sources Science and Technology, vol. 21, no. 4, p. 045007, 2012.

34. L. Dumitran, L. Dascalescu, P. Notingher and P. Atten, "Modelling of corona discharge in cylinder-wire-plate electrode configuration", J. of Electrostat., vol. 65, no. 12, pp. 758-763, 2007.

35. X. Chen, L. Lan, H. Lu, Y. Wang, X. Wen, X. Du and W. He, "Numerical simulation of Trichel pulses of negative DC corona discharge based on a plasma chemical model", Journal of Physics D: Applied Physics, vol. 50, no. 39, p. 395202, 2017.

36. M. Robinson, "A History of the Electric Wind", American Journal of Physics, vol. 30, no. 5, pp. 366-372, 1962.

37. J. Jadidian , M. Zahn, N. Lavesson, O. Widlund, K. Borg, "Effects of impulse voltage polarity, peak amplitude, and rise time on streamers initiated from a needle electrode in transformer oil", IEEE Trans. Plasma Sci. 2012 Mar;40(3) 909-918

38. E. D. Fylladitakis, M. P. Theodoridis and A. X. Moronis, "Review on the History, Research, and Applications of Electrohydrodynamics", IEEE Trans. Plasma Sci., vol. 42, no. 2, pp. 358-375, Feb. 2014.

39. T. Cavallo, A Complete Treatise of Electricity. London, U.K.: Edward, 1777.

40. M. Faraday, "Experimental researches in electricity. Eighth series", Journal of the Franklin Institute, vol. 21, no. 4, pp. 282-286, 1836.

41. J. Maxwell, A treatise on electricity and magnetism. Oxford: Clarendon Press, 2002.

42. J. Moon, D.-H. Hwang, and S.-T. Geum. "An EHD gas pump utilizing a ring/needle electrode", IEEE Trans. Dielectr. Electr. Insul 16:352–58. doi:10.1109/tdei.2009.4815163, 2009

43. W. Qiu, L. Xia, X. Tan, and L. Yang, "The velocity characteristics of a serial-staged EHD gas pump in air", IEEE Trans. Plasma Sci. 38:2848–53. doi:10.1109/tps.2010.2060500, 2010

44. M. Tajmar, "Biefeld-brown effect: misinterpretation of corona wind phenomena", AIAA Journal, vol. 42, no. 2, pp. 315-318, 2004.

45. P. Bérard , D. Lacoste and C. Laux , "Measurements and simulations of the ionic wind produced by a DC corona discharge in air, helium and argon" , 38th AIAA Plasmadynamics and Lasers Conf. (Miami) pp 1–12, 2007

46. D. Harney, "An Aerodynamic Study of the Electric Wind", M.S. thesis, California Institute of Technology, 1954.

47. M. Johnson and B. David "Recent advances in electrohydrodynamic pumps operated by ionic winds: a review." Plasma Sources Science and Technology 26.10 (2017): 103002.

48. L. Zhao and K. Adamiak. "EHD flow produced by electric corona discharge in gases: From fundamental studies to applications (a review)." Particulate Science and Technology 34.1 (2016): 63-71.

49. M. Tabrizchi, T. Khayamian and N. Taj, "Design and optimization of a corona discharge ionization source for ion mobility spectrometry", Review of Scientific Instruments, vol. 71, no. 6, pp. 2321-2328, 2000.

50. M. Rickard and D. Dunn-Rankin, "Numerical simulation of a tubular ion-driven wind generator", J. of Electrostat., vol. 65, no. 10-11, pp. 646-654, 2007.

51. D. Cagnoni, F. Agostini, T. Christen, N. Parolini, I. Stevanović and C. de Falco, "Multiphysics simulation of corona discharge induced ionic wind", J. Appl. Phys., vol. 114, no. 23, p. 233301, 2013.

52. P. Dordizadeh, K. Adamiak and G.S.P. Castle, "Numerical investigation of the formation of Trichel pulses in a needle-plane geometry", J. of Appl. Phys ,vol. 48, no. 41, p. 415203, 2015.

53. J. Poggie, I. Adamovich, N. Bisek and M. Nishihara, "Numerical simulation of nanosecond-pulse electrical discharges", Plasma Sources Science and Technology, vol. 22, no. 1, p. 015001, 2012.

54. S. Chen, J. Nobelen and S. Nijdam, "A self-consistent model of ionic wind generation by negative corona discharges in air with experimental validation", Plasma Sources Science and Technology, vol. 26, no. 9, p. 095005, 2017.

55. M. Ghazanchaei, "Secondary Electrohydrodynamic Flow Generated by Corona and Dielectric Barrier Discharges" (2015). *Electronic Thesis and Dissertation Repository*. 3295.

56. D. Colas, A. Ferret, D. Pai, D. Lacoste and C. Laux, "Ionic wind generation by a wire-cylinder-plate corona discharge in air at atmospheric pressure", J. Appl. Phys., vol. 108, no. 10, p. 103306, 2010.

57. L. Li, S. Lee, W. Kim and D. Kim, "An empirical model for ionic wind generation by a needle-to-cylinder dc corona discharge", J. of Electrostat., vol. 73, pp. 125-130, 2015.

58. M. Naidu, High voltage engineering. Tata McGraw-Hill Education; 2013.

59. J. Feng, "Application of Galerkin Finite-Element Method with Newton Iterations in Computing Steady-State Solutions of Unipolar Charge Currents in Corona Devices", J. Comput. Phys., vol. 151, no. 2, pp. 969-989, 1999.

60. K. Adamiak, V. Atrazhev and P. Atten, "Corona discharge in the hyperbolic point-plane configuration: direct ionization criterion versus approximate formulations", IEEE Trans. Dielectr. Electr. Insul., vol. 12, no. 5, pp. 1025-1034, 2005.

61. N. Sato, "Discharge current induced by the motion of charged particles", Journal of Physics D: Applied Physics, vol. 13, no. 1, pp. L3-L6, 1980.

62. X. Deng, "Numerical Simulation of Corona Discharge in Triode and AC Charger", M.S. thesis, University of Western Ontario, 1997.

63. P. Sattari, G.S.P. Castle and K. Adamiak, "FEM–FCT-Based Dynamic Simulation of Corona Discharge in Point–Plane Configuration", IEEE Trans. Ind. Appl. , vol. 46, no. 5, pp. 1699-1706, 2010.

64. L. Loeb, Fundamental Processes of Electrical Discharge in Gases. NY, John Wiley & Sons, Inc, 1939.

65. A. Meroth, T. Gerber, C. Munz, P. Levin and A. Schwab, "Numerical solution of nonstationary charge coupled problems", J. of Electrostat., vol. 45, no. 3, pp. 177-198, 1999.

66. P. Dordizadeh Basirabad, "Numerical and Experimental Study of the Trichel Pulses in Needle-plane Geometry", Ph.D. dissertation, University of Western Ontario, 2016.

67. K. Adamiak, "Numerical models in simulating wire-plate electrostatic precipitators: A review", J. of Electrostat., vol. 71, no. 4, pp. 673-680, 2013.

68. B. Eliasson, "Basic data for modelling of electrical discharges in gases: oxygen", Asea Brown Boveri Corporate Research Report. 1986:KLR-86 (unpublished).

69. F. Pontiga , C. Soria and A. Castellanos, " Electrical and chemical model of negative corona in oxygen at atmospheric pressure", J. of Electrostat., 1997 Jun 1;40:115-20.

70. L. Zhao and K. Adamiak, "EHD flow in air produced by electric corona discharge in pin–plate configuration", J. of Electrostat. , 2005 Mar 31;63(3):337-50.

71. C. Kim, "Numerical Investigation of Corona Plasma Region in Negative Wire-to-duct Corona Discharge", Aerosol and Air Quality Research, 2010.

72. K. Adamiak and A. Malevanets, "Total Variation Diminishing technique in numerical simulation of Trichel corona in air", J. of Electrostat. , 2017; 87, 110-122.

73. G.M. Colver, S. El-Khabiry, "Modeling of DC corona discharge along an electrically conductive flat plate with gas flow", IEEE Trans. Ind. Appl., Vol.35:2, pp. 387-94, 1999

74. CA. Shi, A. Martynenko, T. Kudra, P. Wells, K. Adamiak, G.S.P Castle,"Electrically-induced mass transport in a multiple pin-plate electrohydrodynamic (EHD) dryer." Journal of Food Engineering 211 (2017): 39-49.

75. Tran T N, Golosnoy I O, Lewin P L and Georghiou G E 2011 Numerical modelling of negative discharges in air with experimental validation J. Phys. D: Appl. Phys. 44 15203

Curriculum Vitae

Name: Sara Mantach

Post-secondary American University of Beirut
Education and   Beirut, Lebanon
Degrees: 2011-2015 B.E.

        The University of Western Ontario
        London, Ontario, Canada
        2016-2018 ME.Sc

Related Work   Electrical Design Engineer
Experience   Adnan Alayan Electro-Mechanical Studies
        2014- 2016

        Teaching Assistant
        The University of Western Ontario
        2016-2018

        Research Assistant
        The University of Western Ontario
        2016-2018

Journal Publication
S. Mantach, K. Adamiak, "A double-vortex EHD flow Patter Generated by Corona Discharge in Point-Plane Geometry." Journal of Electrostatics (Accepted for publication)

Conference Presentations
S. Mantach, K. Adamiak, "Validity of Kaptzov's Hypothesis in Numerical Simulation of Corona Discharge Problems", submitted to 11eme Conference de la Societe Franciase d'Electrostatique
S. Mantach, K. Adamiak, "A full EHD Flow Pattern in Point-Plane Corona Discharge", submitted to 2018 Electrostatics Joint Conference - ESA